Estuarine, Coastal and Shelf Science (1998) **47**, 769–795
Article No. ec980387

Inverse-estuarine Features of the Upper Gulf of California

M. F. Lavín, V. M. Godínez and L. G. Alvarez

Departamento de Oceanografía Física, CICESE, Ensenada, Baja California, México

Received 14 April 1998 and accepted in revised form 12 June 1998

The Upper Gulf of California is the shallow (depth <30 m), tidal area at the head of the Gulf of California. It is an inverse estuary, due to the high evaporation rate ($E \sim 1{\cdot}1$ m year^{-1}) and almost nil freshwater input from rainfall and the Colorado River. Historical and recent hydrographic data show that the area is almost vertically well-mixed throughout the year, that the horizontal distribution of properties follows the bathymetry, and that the hydrography has a strong annual modulation. As in other negative estuaries, the year-round salinity increase toward the head causes the density to do likewise, despite the seasonally reversing temperature gradient. The pressure gradient thus formed leads to water-mass formation and gravity currents (speed $\sim 0{\cdot}1$ ms^{-1}), both in winter and in summer. In winter, the high salinity water sinks beyond 200 m, while in summer it only reaches a depth of 20–30 m. The gravity currents appear to be modulated by the fortnightly tidal cycle, with events in neap tides. This phenomenon causes the presence, at least during neap tides, of slight stratification ($\Delta\sigma_t \approx -0{\cdot}2$).

Keywords: inverse estuaries; gravity currents; warm semi-enclosed seas; Mexico coast

Introduction

The Upper Gulf of California (Figure 1), henceforth abbreviated UGC, is the shallow northernmost part of the Gulf of California. It has a triangular shape, bound by the 30 m isobath and the converging coast of mainland México and the Baja California Peninsula. It is a highly tidal sea, with maximum spring tidal amplitude of about 5 m, and tidal current speeds exceeding 1 ms^{-1} (Alvarez Sánchez *et al.*, 1993). It now enjoys a Biosphere Reserve status, for it is the home of indigenous endangered species (*Totoaba macdonaldi* or Totoaba, and *Phocoena sinus* or Vaquita), as well as a zone of reproduction and nursery ground for many others, including some of economical importance. The management of the resources of the UGC will be hampered by a lack of basic knowledge about the physical environment. The little that is known about the oceanography of the UGC by direct observation is based in hydrographic data collected almost monthly between October 1972 and September 1973 (Alvarez-Borrego *et al.*, 1973). This is what is known, from those observations, at present:

(1) Surface temperature increases to the NW in summer and decreases in winter. Temperature maxima (~ 32 °C) are attained in August, and minima (~ 8 °C) in December (Alvarez-Borrego & Galindo-Bect, 1974; Alvarez-Borrego *et al.*, 1975).
(2) Surface salinity always increases to the NW, with a seasonal maximum (39) in May-September and minimum (37) in December-February (ibid).
(3) The UGC is vertically well-mixed throughout the year (Organista Sandoval, 1987; Martínez Sepúlveda, 1994).
(4) The front between the vertically well-mixed regime of the UGC and stratified conditions is found about the 30 m isobath in summer, and that of ~ 60 m in winter (Argote *et al.*, 1995).

Features (1) and (2) can readily be observed in Figure 2. Based on the pattern of the surface distributions of salinity and temperature, a cylonic residual circulation has been proposed for the UGC (Alvarez-Borrego & Galindo-Bect, 1974). Only the surface distributions were described by Alvarez-Borrego and Galindo-Bect (1974) and Alvarez-Borrego *et al.* (1975). Indeed not even the distribution of surface density has been described, and Figure 2 shows the so-far unnoticed (and very interesting) fact that density increases toward the NW both in winter and summer.

By numerical modelling, the following has been proposed:

(1) Tidal mixing is responsible for maintaining the summer-time well-mixed conditions of the UGC, and therefore controls the summer position of the mixing front. In winter, vertical convection is added to tidal

0272-7714/98/120769+27 $30.00/0

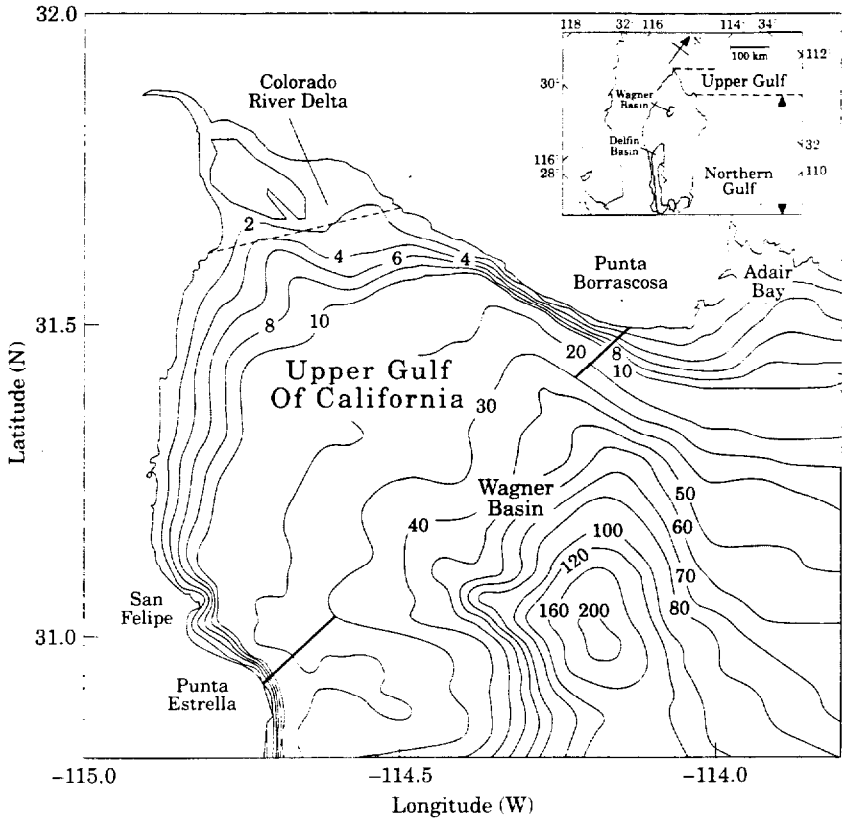

FIGURE 1. Bathymetry of the Upper Gulf of California (UGC), taken here as the area with bottom depth less than 30 m, to the NW of a line between Punta Estrella and Punta Borrascosa. Depth in metres.

mixing in controlling the front location (Argote *et al.*, 1995).

(2) The predicted circulation in the UGC due to topographic tidal rectification is different for different models. According to Argote *et al.* (1998) there is a convergence at the Delta, and a southward compensating jet along the axis. Marinone (1997) finds a cyclonic circulation. Carbajal *et al.* (1997) do not obtain a well-defined circulation. In all cases the residual speeds are of O (0·01 ms^{-1}). These numerical results are very sensitive to the bathymetry, to the grid resolution and to the friction coefficient; also they are very difficult to verify by observation.

(3) The wind, which blows from the NW in winter and from the SE in summer, induces a cyclonic residual circulation in winter and an anticyclonic circulation in summer, of O (0·02–0·03 ms^{-1}) (Carbajal, 1993; Beier, 1997; Argote *et al.*, 1998). No data are available to support any of these numerical results for the UGC, although they agree with observations made just south of the UGC, in Delfin Basin (Lavín *et al.*, 1997; Argote *et al.*, 1998).

In this paper historical and recent hydrographic data are used to make an updated description of the hydrography of the UGC, including vertical structure and its seasonal variability. Water mass formation is also discussed and observations of gravity currents shown.

Observations

The study area

The bathymetry on the peninsular side has a gently sloping bottom and, in the mean, is shallower than the mainland side, where the bottom depth rapidly reaches the maximum of the cross-section, in a channel or canyon that extends to the 200 m-deep Wagner Basin. The natural southern limit of the UGC is the front separating the vertically well-mixed coastal waters of the UGC and the stratified waters of Wagner Basin. As mentioned before, the 30 m isobath marks the approximate summer position of that front, and therefore is a convenient sea-boundary or limit of the UGC.

Historical data

The historical data were collected approximately monthly between October 1972 and September 1973;

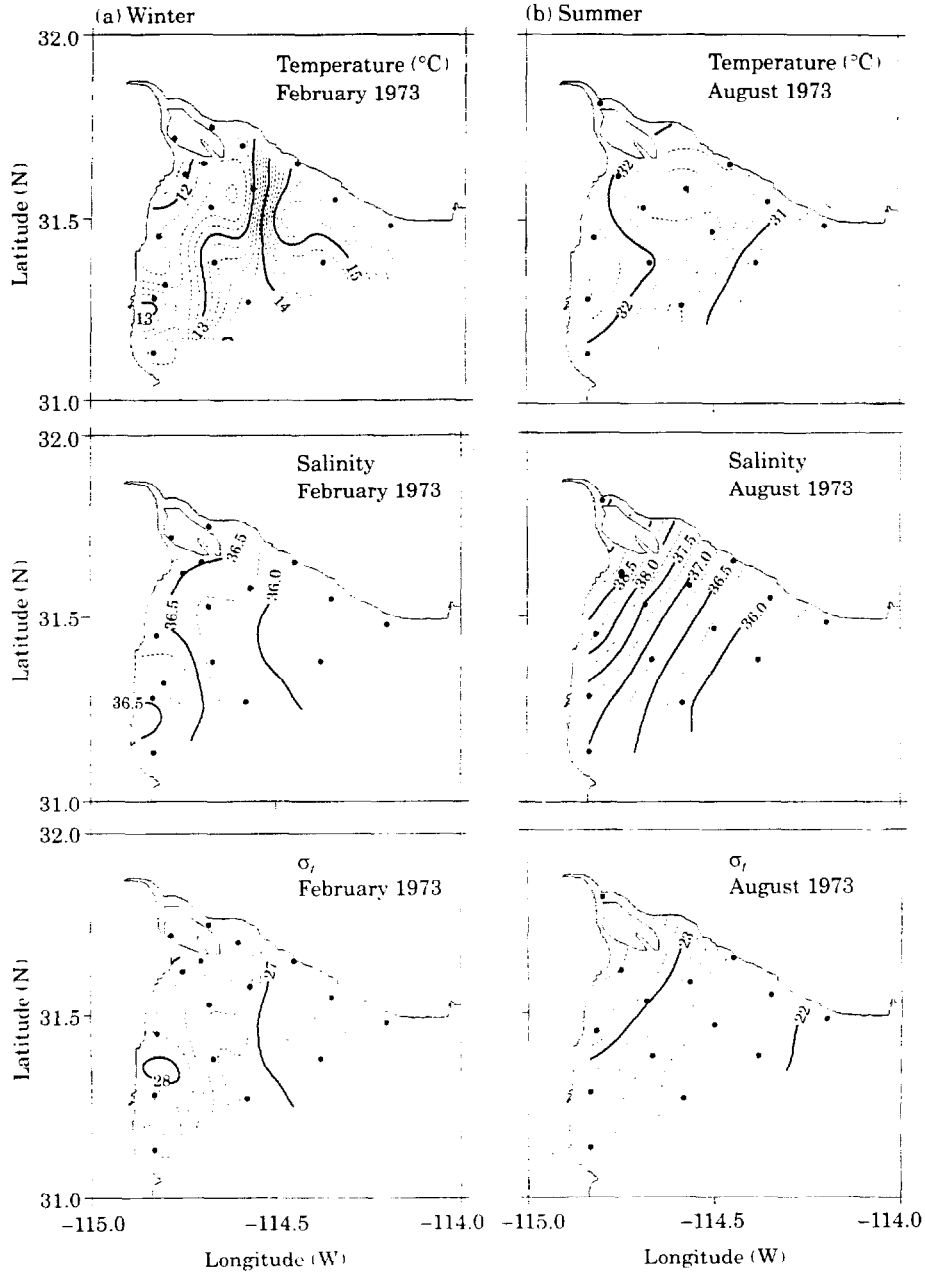

FIGURE 2. Surface distribution of temperature, salinity and σ_t from the historical data. Two examples are shown: (a) winter (February 1973) and (b) summer (August 1973).

typical station coverage is shown by the dots in Figure 2, and Figure 3(a) shows the position of all the stations. The October 1972 data are not used here because of unusual rainy conditions; the full set of data can be found in the report by Alvarez-Borrego *et al.* (1973). Although this is the only data set available and covers a full annual period, it has some limitations. The data were collected with bottles and reversing thermometers only at 0, 5 and 10 m; therefore the bottom layer was not sampled in a very wide area where the bottom depth exceeds 10 m (see Figure 1). The station separation is quite large, with only three across-gulf rows of four stations each in the main body of the UGC.

New data

CTD data were obtained in the UGC on seven separate occasions between December 1993 and July

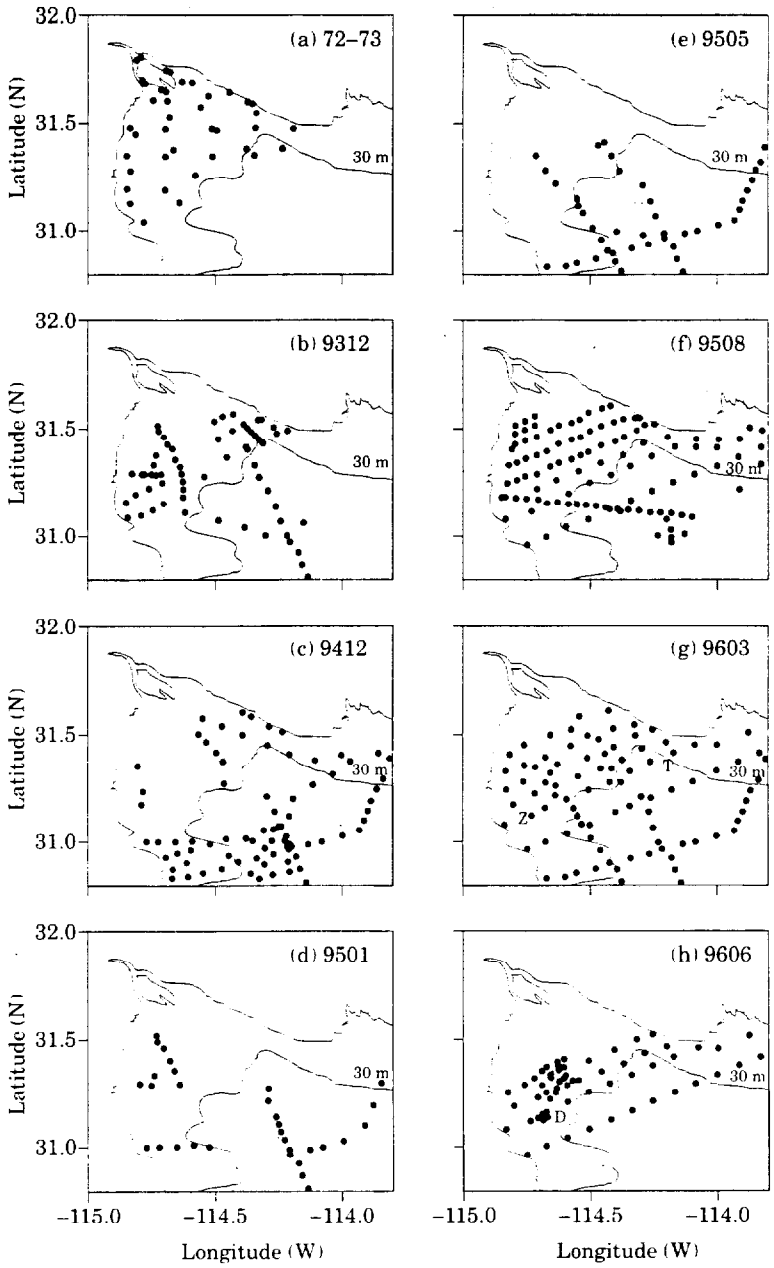

FIGURE 3. (a) Positions of the stations of the historical data. (b) to (h) Positions of the CTD stations made between December 1993 and June 1996. The surveys are named according to the year and month when they took place (e.g. 9606 = June 1996). The sites of time-series measurements are marked as follows: in 9603 (g), the current meter mooring sites are marked by Z and T. In 9606 (h), the current meters were moored at site D, two CTD time series were also made at site D, one at spring and one at neap tides.

1996, always from the BO *Francisco de Ulloa*. The station separation [Figure 3(b)–(h)] is smaller than in the historical data, but full coverage of the UGC was not always achieved; in fact, no data were collected in the Delta. Some of the across-UGC lines of stations intersect the deeper-than-30 m channel in the mainland side, and it will be seen that stratified conditions are almost always encountered there, with clear near-bottom intrusions of water from Wagner Basin. The data from the best sampled surveys will be presented in some detail, in a constructed annual cycle. The full data set, including the points in Figure 3 that fall outside the UGC, will be used in the T/S diagram. All the CTD surveys were made in neap tides, so that the vessel could venture as far north as it did.

TABLE 1. Details of current meter installations in the Upper Gulf of California during March and June 1996

Site ↓	Lat. (°N)	Long. (°W)	Bottom depth (m)	CM height (m)	δt (min) ΔT (days)	START (hh:mm dd/m/yy)	END (hh:mm dd/m/yy)	S/N
Z	31·14	114·67	22	5	20	17:40	12:00	AA
					3·76	26/3/96	29/3/96	11653
T	31·40	114·19	25	5	20	00:00	16:00	GO
					14·66	26/3/96	09/4/96	489
D	31·14	114·67	22	1	10	19:30	08:40	AA
Neaps					2·54	23/6/96	26/6/96	11653
D	31·14	114·67	22	6	10	19:50	08:30	GO
Neaps					2·52	23/6/96	26/6/96	489
D	31·14	114·67	22	1	10	06:20	08:10	AA
Springs					4·07	28/6/96	01/7/96	11653
D	31·14	114·67	22	6	10	07:00	06:40	GO
Springs					3·98	28/6/96	01/7/96	489

The sampling rate is δt (minutes), and the length of the time series is ΔT (days). GO, General Oceanics; AA, Aaanderaa.

In the survey made in December 1993 (coded as 9312), a Neil-Brown Smart CTD was used; its field and laboratory calibrations are reported by Godinez *et al.* (1995). In all the other surveys a factory-calibrated SBE-911*plus* CTD was used, and the data were processed using the manufacturer's software, as detailed by Garcia *et al.* (1995); data interpolated to 2 m intervals are used here. The current meters used were either Aanderaa RCM-7 or General Oceanics Niskin 6011 Mark II (tilt-type).

Time series

Time-series measurements were made in the 9603 and 9606 surveys. In March 1996, hourly time-series of CTD casts were made with the ship anchored at a place north of San Felipe [marked Z in Figure 3(g)] during neap and springs tides. Current meters were installed in March of 1996 at the positions marked by T (25 m of water) and Z (22 m) in Figure 3(g), both at 5 m above the bottom; the instrument at Z worked for only 3 days, and that at T (mainland side) sampled for 15 days. In June of 1996, current meter (at 1 m and 6 m above the bottom) observations and half-hourly CTD casts were made again North of San Felipe; the site is marked by D (water depth 22 m) in Figure 3(h). The time-series are 53 h long in spring tides and 58 h long in neap tides. Winds were measured at Punta Estrella (Figure 1), South of San Felipe, throughout 1995 and 1996. Table 1 summarizes the details of the current meter deployments.

Results

T/S diagrams

The T/S diagrams for the historical and new data sets [Figures 4(a),(b)] illustrate many of the features of the hydrography of the UGC. The apparent differences between the two data sets are due to differences in the surveyed areas: the historical data are only from the top 10 m, the new set does not include data from the Delta, but includes many profiles from Wagner Basin, and one from Delfín Basin, in order to put the UGC data in a regional perspective.

The seasonal cycle of the temperature is the most obvious feature: the surface layer temperature changes from about 15 °C in January to about 31 °C in August. The increase of temperature toward the shallower (saltier) water in summer and its crease in winter is also apparent. There is also a clear seasonal signal in salinity, with the maximum in August and minima from December to March. In addition to the seasonal signal of the density, the increase of density toward the shallowest (saltiest) water throughout the year is discernible. The water in the UGC is densest in December, January and February.

Hydrography and currents

In this subsection, the annual cycle of the hydrographic structure of the UGC is described, based on the best-sampled surveys of the new data set. Some limited but interesting current measurements are also presented. In the remainder of this paper, surface and

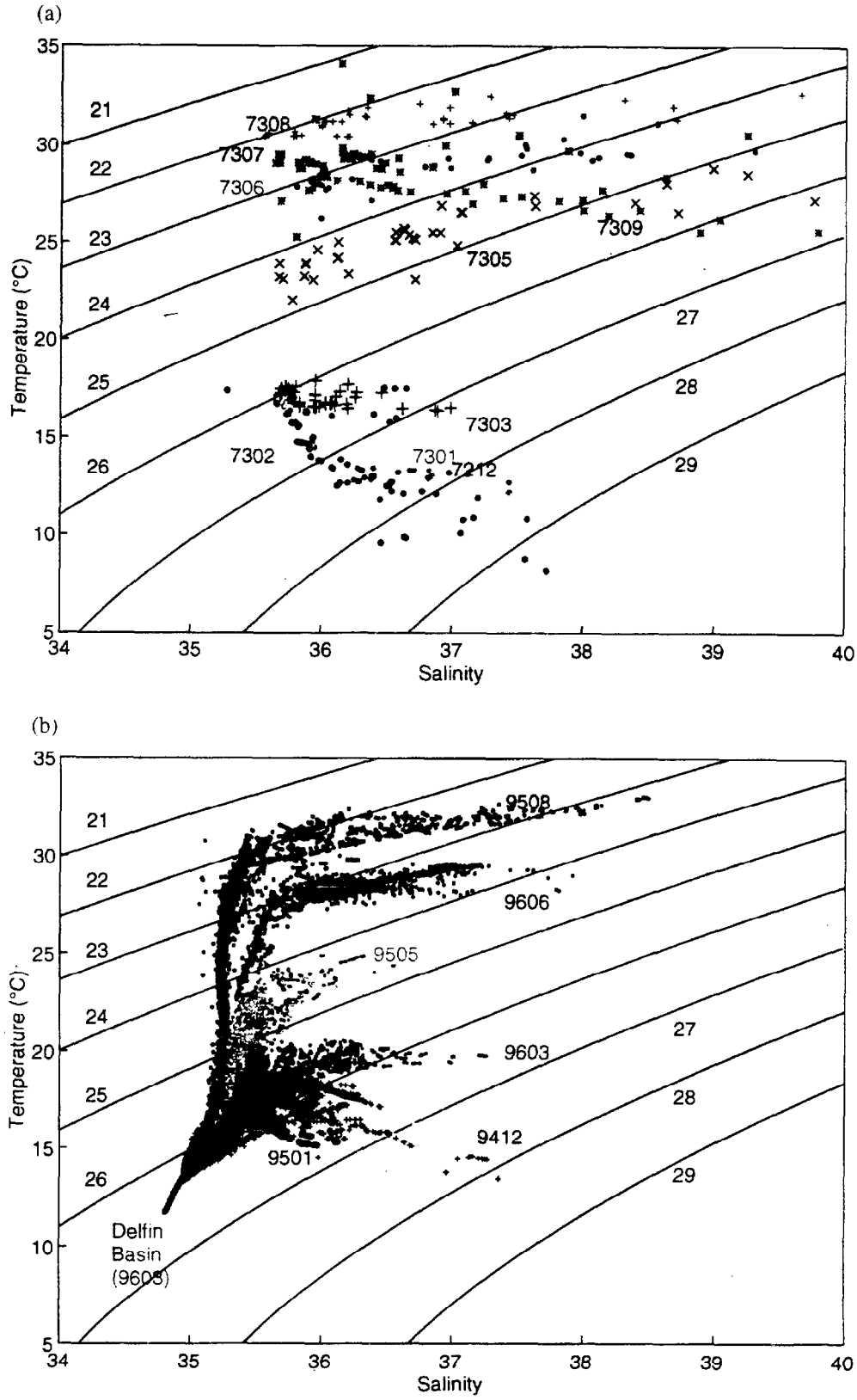

FIGURE 4. Temperature-Salinity diagrams for the Upper Gulf of California: (a) Historical data from December 1972 to September 1973 and (b) Data obtained between December 1993 and July 1996. The salinity of the historical data is in ppt and the new data is in ups; units are omitted in both cases.

bottom values of variables like temperature (T), salinity (S) and density (σ_t) will be denoted by subindices *s* and *b*, respectively. The difference of the surface minus the bottom values will be denoted by Δ (e.g. $\Delta T = T_{s-T_t}$).

Winter (7–17 December 1993). The distributions of temperature, salinity and σ_t [Figure 5(a),(b),(c)] show the pattern observed previously in the historical data, with the coldest (~ 15 °C), saltiest (36·7) and densest (27·2) water in the shallow, extended shelf on the peninsula side. The entire UGC was vertically homogeneous in the three variables [Figure 5(d),(e),(f)].

Spring (25 March to 9 April 1996). The distribution of surface salinity [Figure 6(a)] shows the increase toward the NW, where the maximum salinity (37·2) is found in a nucleus close to the Baja California (henceforth BC) coast. Adair Bay has salinity above 36. The distribution of ΔS [Figure 6(b)] shows vertical homogeneity almost throughout the UGC. The vertical contours of salinity (Figure 6) show that the high salinity nucleus is vertically homogeneous, except at the seaward edge, where $\Delta S \sim 0{\cdot}1$ [Figure 6(b)]. The tilt of the isohalines at the edge of the nucleus suggests that it extends as a near-bottom intrusion, with salinity decreasing outwards. At the eastern end of Line S4 there is an increase of salinity near the bottom, which may have originated further north, or locally in Adair Bay; this latter suggestion seems to be supported by the distributions of salinity at the eastern end of Lines S5 and S6.

The distribution of T_s [Figure 7(a)] shows that the coastal water has begun to warm, with the distribution pattern in transition from winter to summer conditions. A streak of minimum temperature is found in the middle of the UGC. ΔT [Figure 7(b)] shows stable stratification in the UGC, of about 0·2 °C, while in Adair Bay the temperature profile is inverted with $\Delta T \sim -0{\cdot}1$ °C. The vertical cross-sections (Lines S1 to S4) show that the sites with high salinity water described above are also warm, both in the NW off BC and in Adair Bay. In the T and S fronts off BC, in lines S5 to S6, the isotherms tilt in opposition to the isohalines. The eastern end of Line S4 presents a temperature increase near the bottom, coinciding with the salinity increase. Extensive temperature stratification is present only in Lines S5 and S6. The boundary between the stratified and well-mixed areas is given approximately by the $\Delta T = 1$ °C isoline [Figure 7(b)], and coincides quite well with the frontal position predicted by Argote *et al.* (1995).

The distribution σ_{ts} [Figure 8(a)] shows that the densest water ($\sigma_t \sim > 26{\cdot}1$) is found at the NW corner of the UGC. $\Delta\sigma_t$ shows [Figure 8(b)] slight stratification ($\Delta\sigma_t \sim -0{\cdot}15$) in most of the UGC, with no inversions. The vertical cross-sections of density (Figure 8) follow very closely the salinity sections, the density maxima coinciding with the salinity maxima. The distribution of water with $\sigma_t > 26{\cdot}8$ (shaded in Figure 8) from Line S1 to Line S4 suggest that the densest water originated in the shallow BC side and moved as a near-bottom intrusion as far as Line S4. There is no water with $\sigma_t > 26$ elsewhere in the UGC.

The tides, currents and wind measurements made during this survey are shown in Figure 9. The tidal range in San Felipe varied from less than 1 m to almost 6 m [Figure 9(a)]. The currents measured at site T (black squares in Line S5, previous three figures) show [Figure 9(b)] tidal currents that reach 0·5 ms^{-1}, while the low-passed flow is only 0·04 ms^{-1} at its maximum [Figure 9(e)], which occurred during neap tides and was directed out of the UGC. The current meter data from the peninsula side (site Z) lasted too little to allow filtering [Figure 9(c)], but the fact that the flood is slower than the ebb suggests southward residual flow. There is no obvious correlation between the residual currents and the wind [Figure 9(f)]. The CTD time-series made at site Z (not shown) reveal well-mixed conditions both in spring and neap tides, with some near-surface temperature stratification in the afternoon.

Early summer (23 June to 1 July 1996. The shallowest sections, S1 and S2 were not sampled in this cruise, therefore the authors have only the three lines at the entrance to the UGC and S6, which passes through the edge of Wagner Basin.

The surface salinity [Figure 10(a)] increases from 35·6 in the entrance to over 36 in Adair Bay and up to 36·7 off the BC coast. In the BC zone there is a very pronounced salinity inversion (defined here as salinity increasing downward, which is the inverse of the normal vertical salinity variation in the Gulf of California) [Figure 10(b)], with the bottom salinity exceeding surface salinity by up to 0·5. The vertical sections of salinity S3 and S4 (Figure 10) show that the salinity inversion off BC is due to high salinity water from the coast extending over the bottom to the south and east, in what looks like a gravity current. In vertical sections S5 and S6, water with salinity between 36 and 37 hugs the BC coast, with the tilt of the isohalines decreasing to the south. There is also some high salinity water (>36) on the Eastern end of line S5 (Adair Bay), and also at the bottom on the eastern end of Line S4; the source of this bottom water is probably Adair Bay. The central part of sections S6, S5 and S4 have lower salinity (35·4),

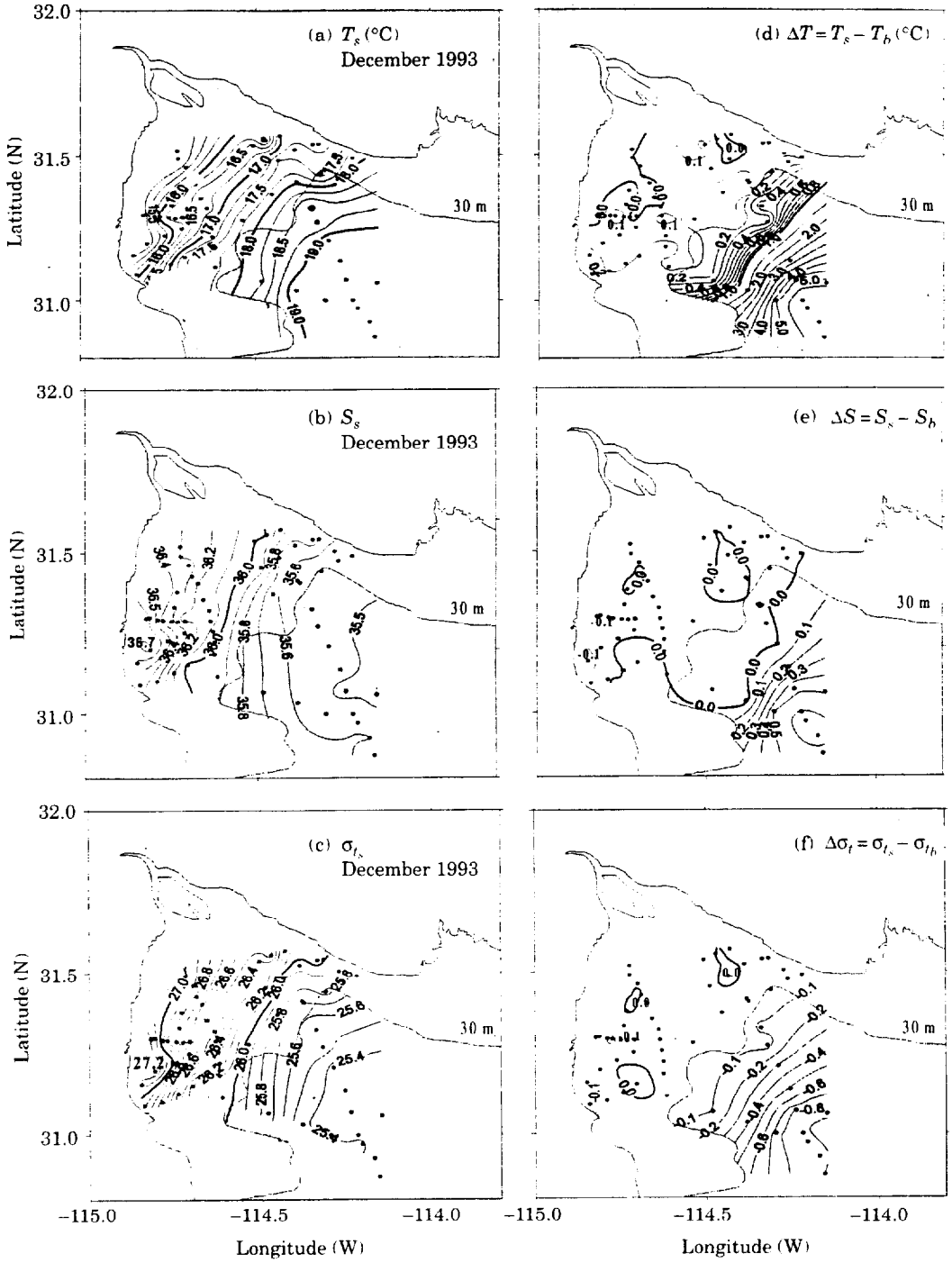

FIGURE 5. Hydrography of the UGC in December 1993: (a) surface temperature T_s; (b) surface salinity S_s; (c) surface σ_t; (d) surface to bottom temperature difference $T_s - T_b$; (e) surface to bottom salinity difference $S_s - S_b$; (f) surface to bottom density difference bottom density difference $\sigma_{t_s} - \sigma_{t_b}$. Areas deeper than 30 m is shaded.

indicating the influence of water from Wagner Basin.

The surface temperature [Figure 11(a)] shows the summer pattern, with the highest temperatures (29 °C) in the shallowest zone and the lowest (25 °C) at the entrance to the UGC. The ΔT distribution [Figure 11(b)] shows that the area off BC that had the salinity inversion also is inverted in temperature, with bottom water up to 0·5 °C warmer than that at the surface. Figure 11(b) also shows that the tidal mixing

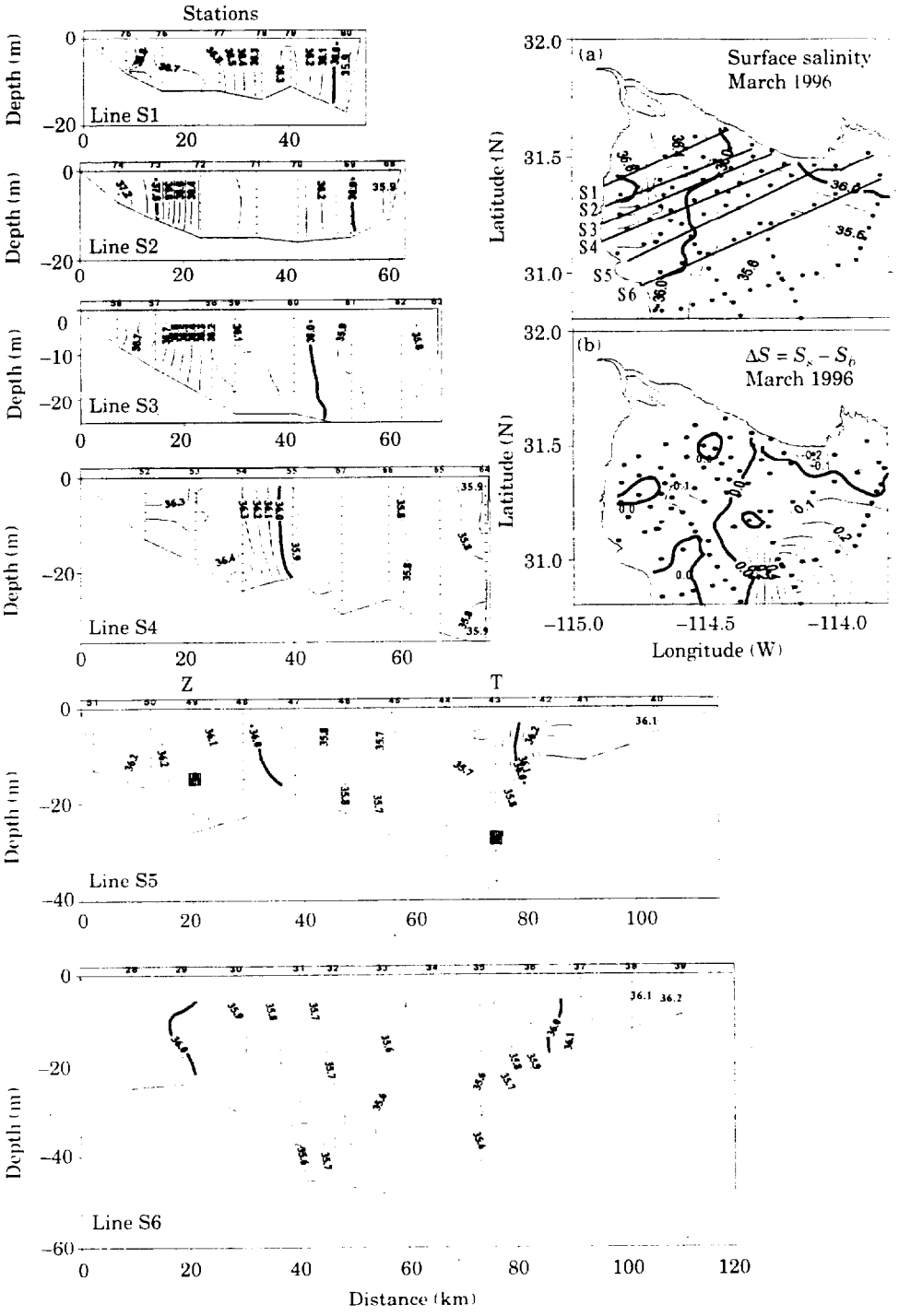

FIGURE 6. Distribution of salinity in the Upper Gulf of California in March 1996: (a) surface salinity; (b) surface to bottom salinity difference. Line S1 to Line S6: vertical cross-sections of salinity along the cross-gulf lines marked in (b). The black squares in Line S5 show the position of the current meters.

front (defined by $\Delta T = 1\ ^{\circ}C$) is approximately at the same position as in spring. The vertical distributions of temperature (Lines S3 to S6, Figure 11) show that the isotherms off BC have the same tilt as the isohalines in the previous figure. The central part is influenced by cold, less salty water from Wagner Basin, while the BC coast and Adair Bay contain the warmest and saltiest water.

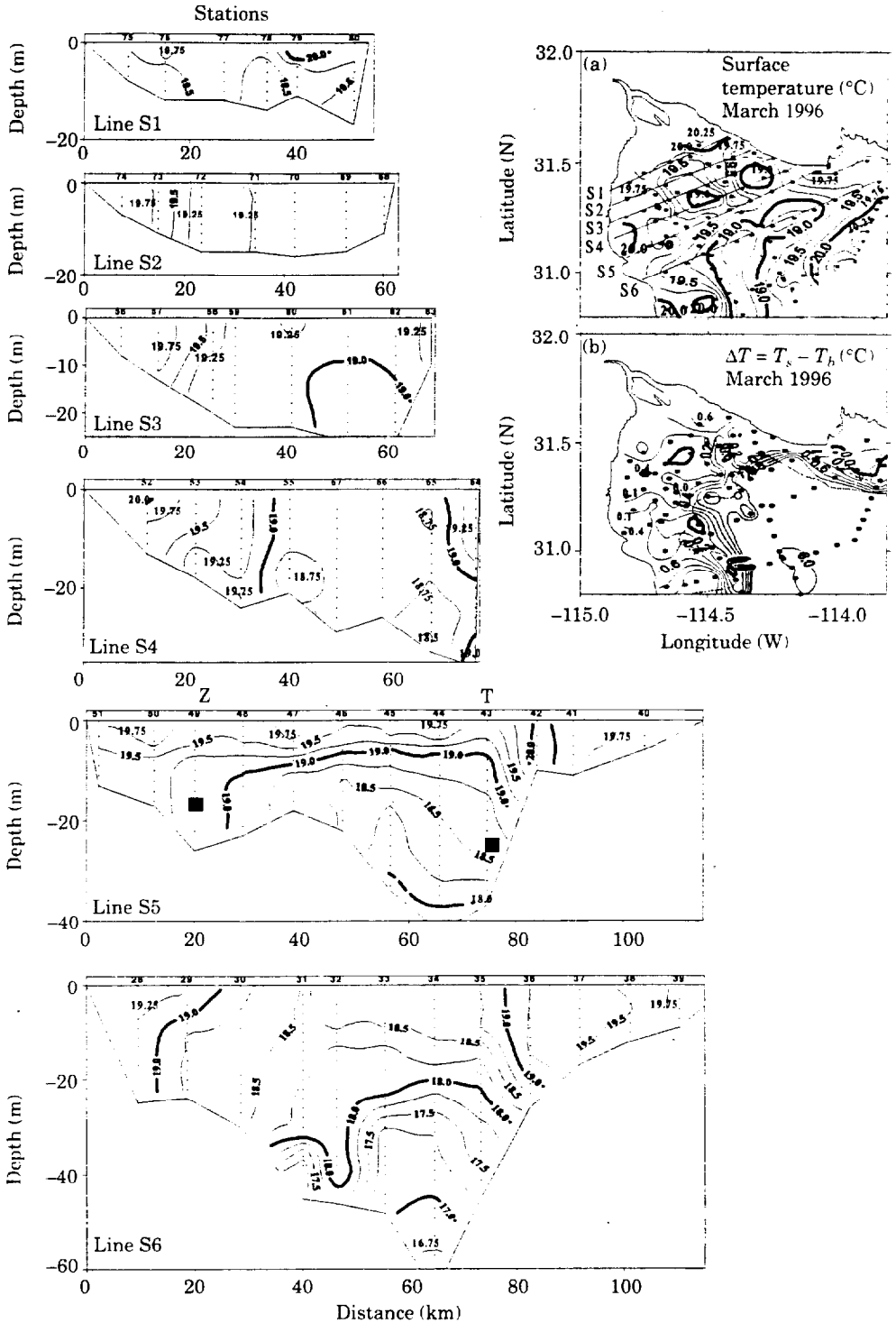

FIGURE 7. Distribution of temperature in the Upper Gulf of California in March 1996: (a) surface temperature; (b) surface to bottom temperature difference. Line S1 to Line S6: vertical cross-sections of temperature along the cross-gulf lines marked in (b). The black squares in Line S5 show the position of the current meters.

There is very little variation in surface σ_t [Figure 12(a)], with maxima in the coastal water off BC (23·4) and in the water from Wagner Basin at the centre of the entrance (23·6). All the area was stably stratified, with values of $\Delta\sigma_t$ up to $-0{\cdot}2$ in the UGC, and up to $-0{\cdot}6$ in the edge of Wagner Basin

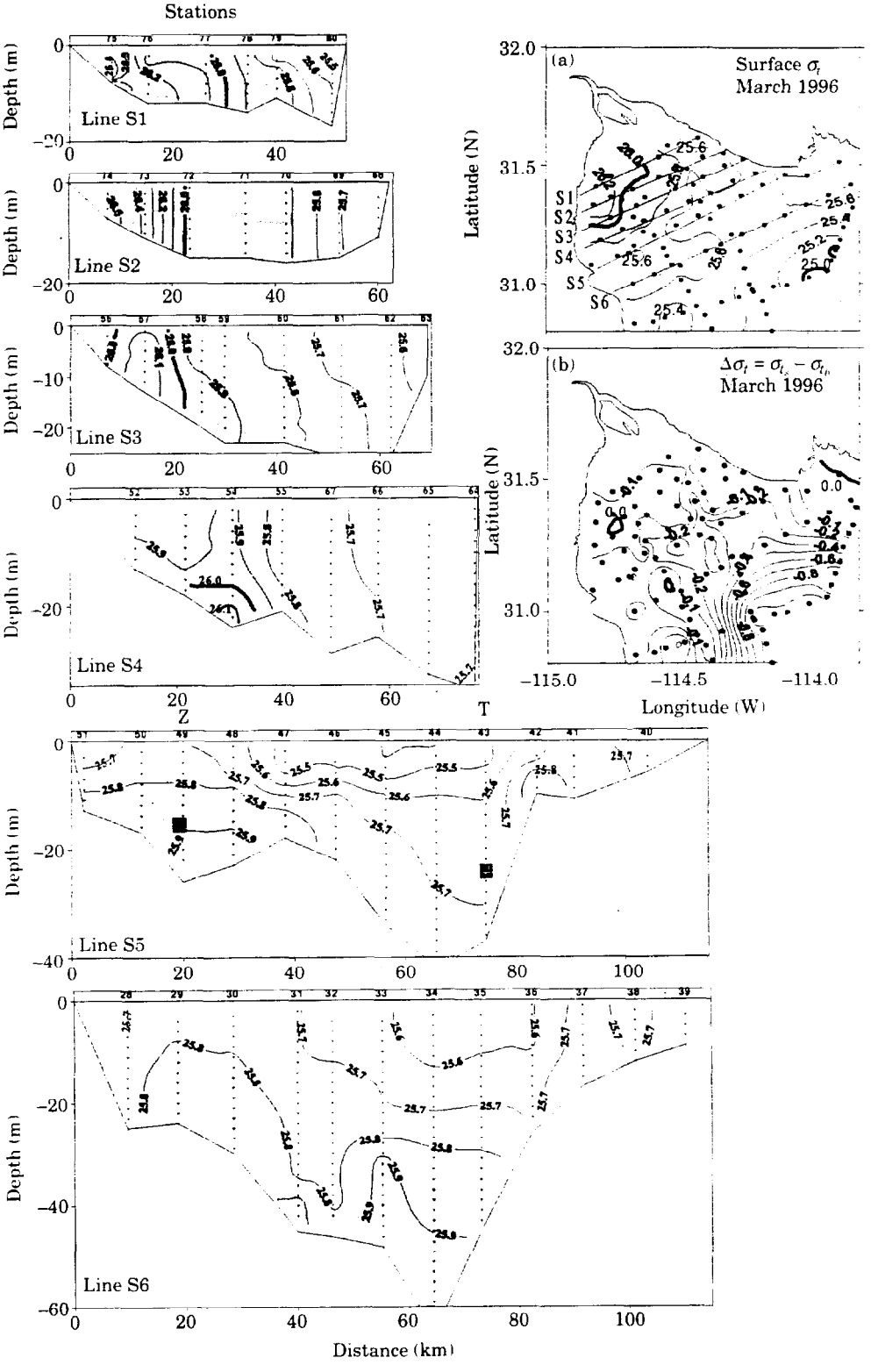

FIGURE 8. Distribution of σ_t in the Upper Gulf of California in March 1996: (a) surface σ_t; (b) surface to bottom σ_t difference. Line S1 to Line S6: vertical cross-sections of σ_t along the cross-gulf lines marked in (b). The black squares in Line S5 show the position of the current meters.

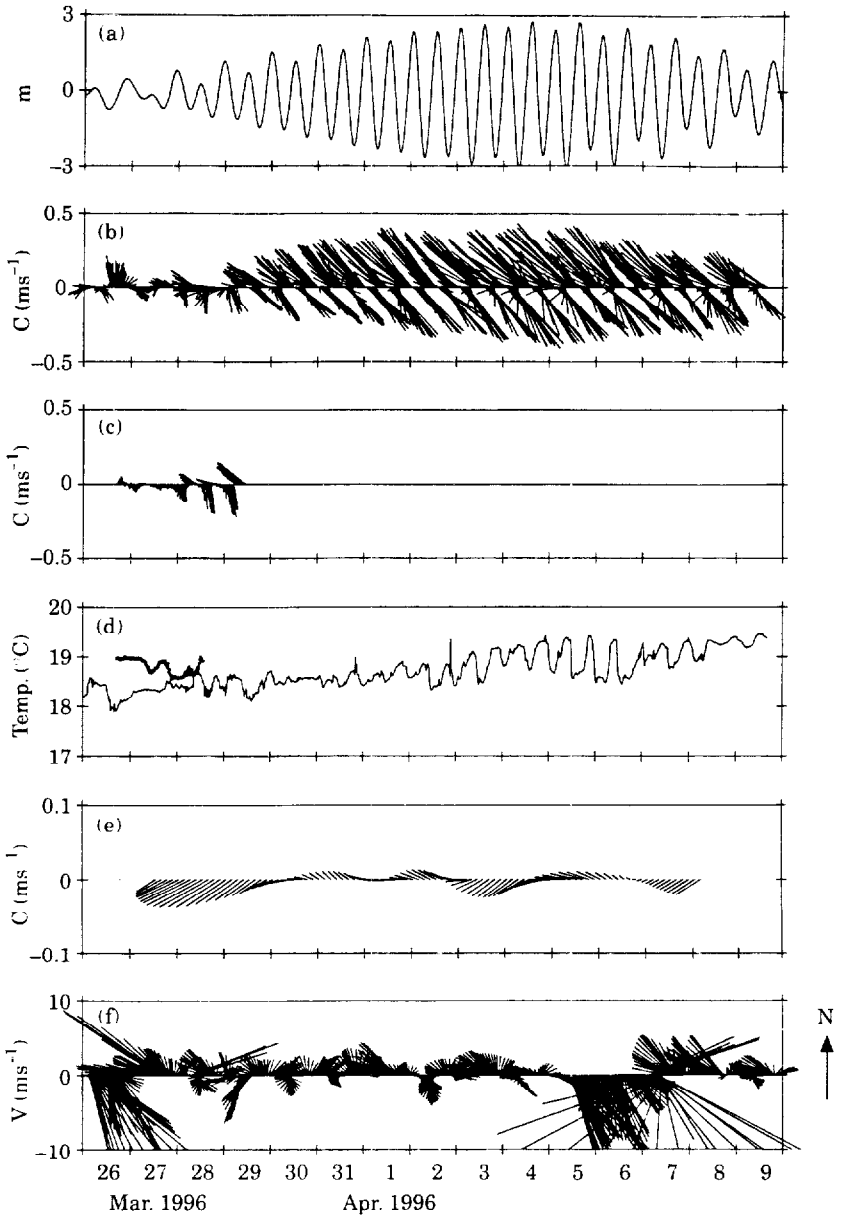

FIGURE 9. Time-series collected in the UGC between 26/03/96 and 09/04/96: (a) tidal height at San Felipe; (b) current velocity vectors 1 m above the bottom at site T; (c) current velocity vectors 1 m above the bottom at site Z; (d) water temperature measured by the current meters at site T (thin line) and site Z (thick line); (e) low-passed current velocity vectors at site T; (f) wind velocity vectors at Punta Estrella (Figure 1), drawn in oceanographic convention.

[Figure 12(b)]. The vertical distribution of density (Lines S3 to S6, Figure 12) reflects the salinity distribution in the West, and the temperature distribution in the deeper, central part. Although the isopycnals on the BC side of Lines S3 to S5 have the same inclination as the isohalines and the isotherms, the vertical gradients are not as strong; this is due to the opposing effects of both salinity and temperature increasing toward the bottom. In all the sections there is a zone of minimum density, sandwiched between the BC coastal high density (due to salt) and the offshore high density (due to temperature) water from Wagner Basin.

The neaps CTD time series [Figure 13(a)] was made on the edge of the patch of high salinity water (Site D Line S5, Figure 12), just before sampling the grid of stations. Initially the water was homogeneous ($T \approx 29{\cdot}4$ °C, $S \approx 36{\cdot}9$, $\sigma_t \approx 23{\cdot}4$), but soon became stratified with the appearance in the surface, of less dense, less warm and less salty water ($T \approx 28{\cdot}2$ °C,

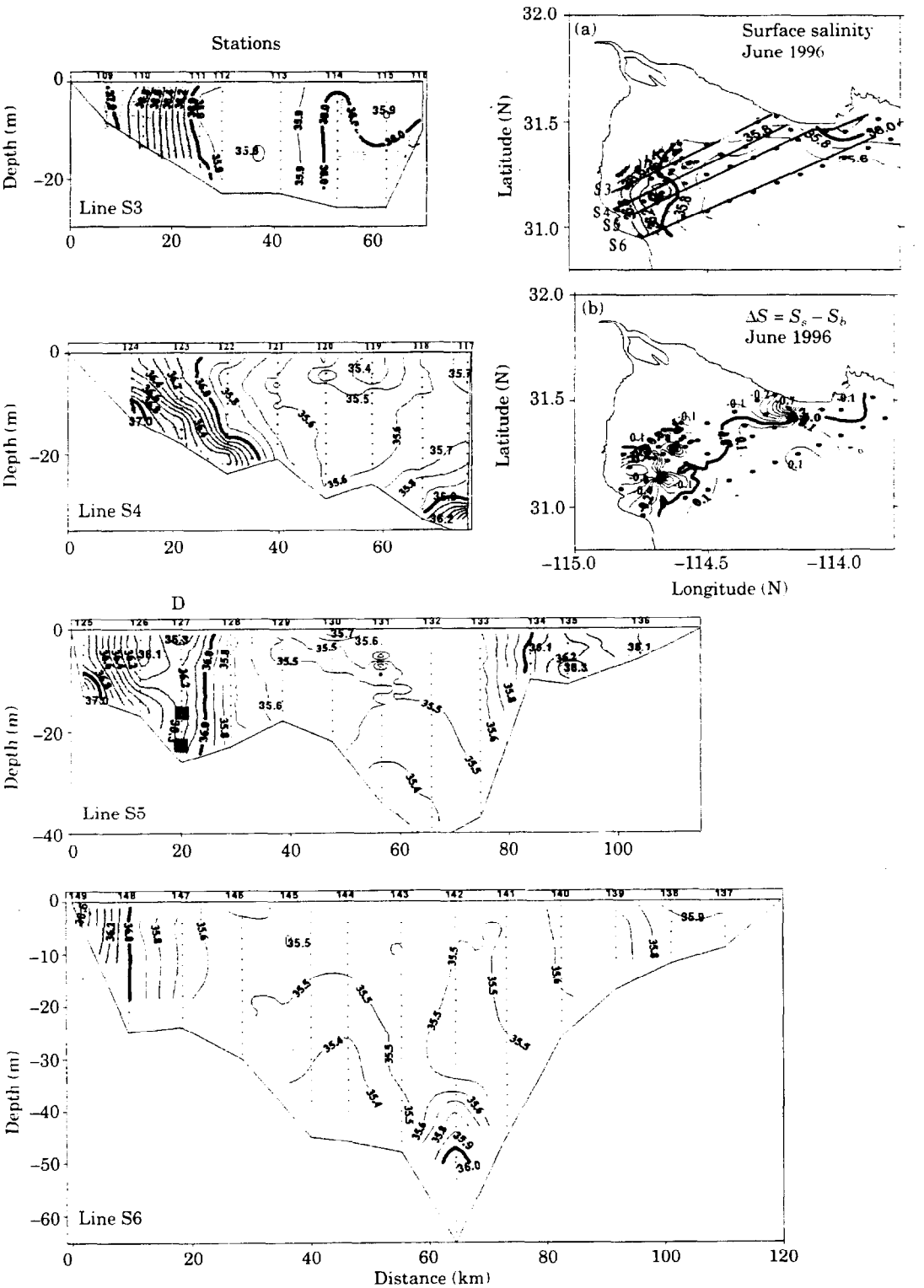

FIGURE 10. Distribution of salinity in the Upper Gulf of California in June 1996: (a) surface salinity; (b) surface to bottom salinity difference. Line S3 to Line S6: vertical cross-sections of salinity along the cross-gulf lines marked in (a). The black squares in Line S5 (Site D) show the position of the current meters.

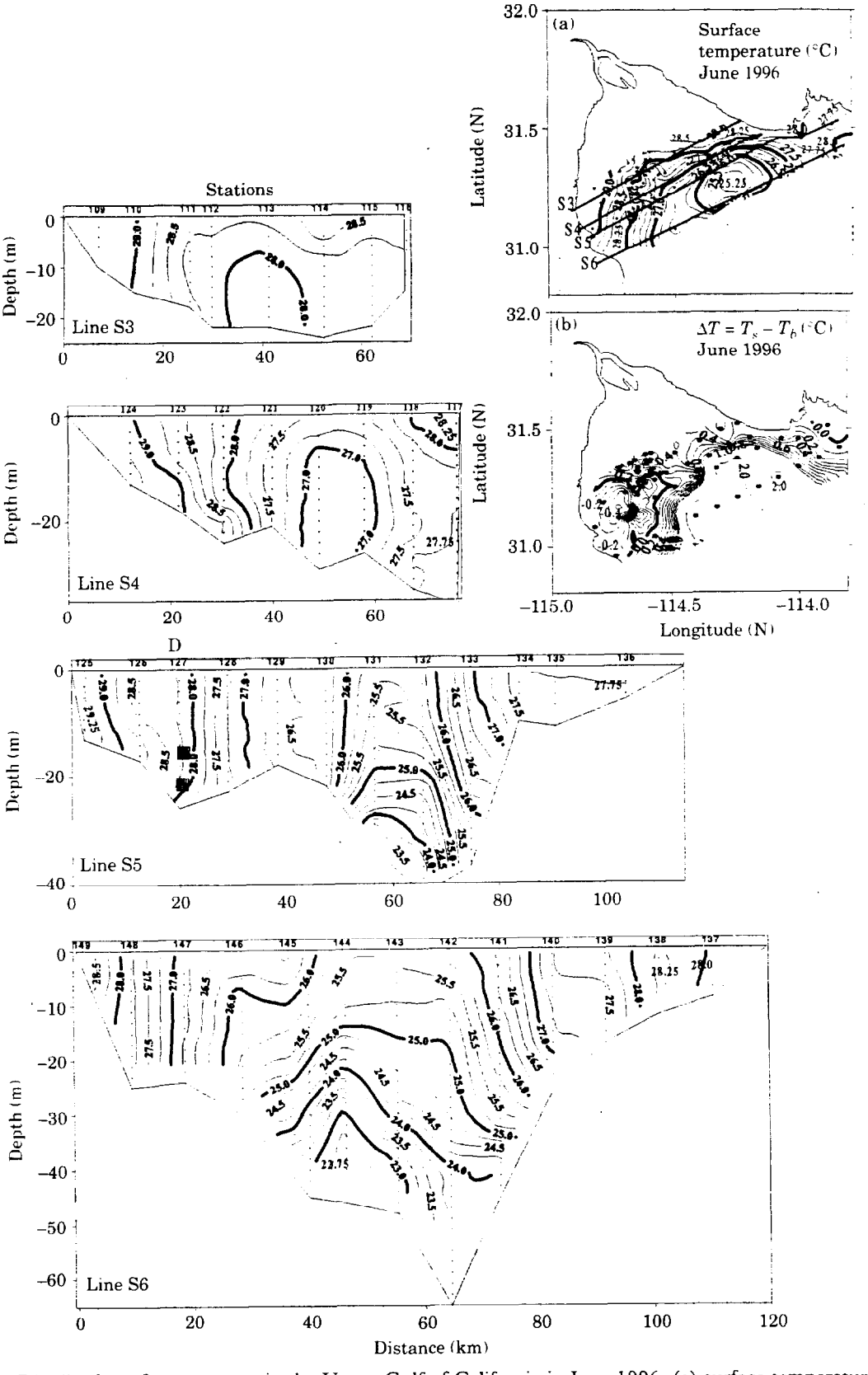

FIGURE 11. Distribution of temperature in the Upper Gulf of California in June 1996: (a) surface temperature; (b) surface to bottom temperature difference. Line S3 to Line S6: vertical cross-sections of temperature along the cross-gulf lines marked in (a). The black squares in Line S5 (Site D) show the position of the current meters.

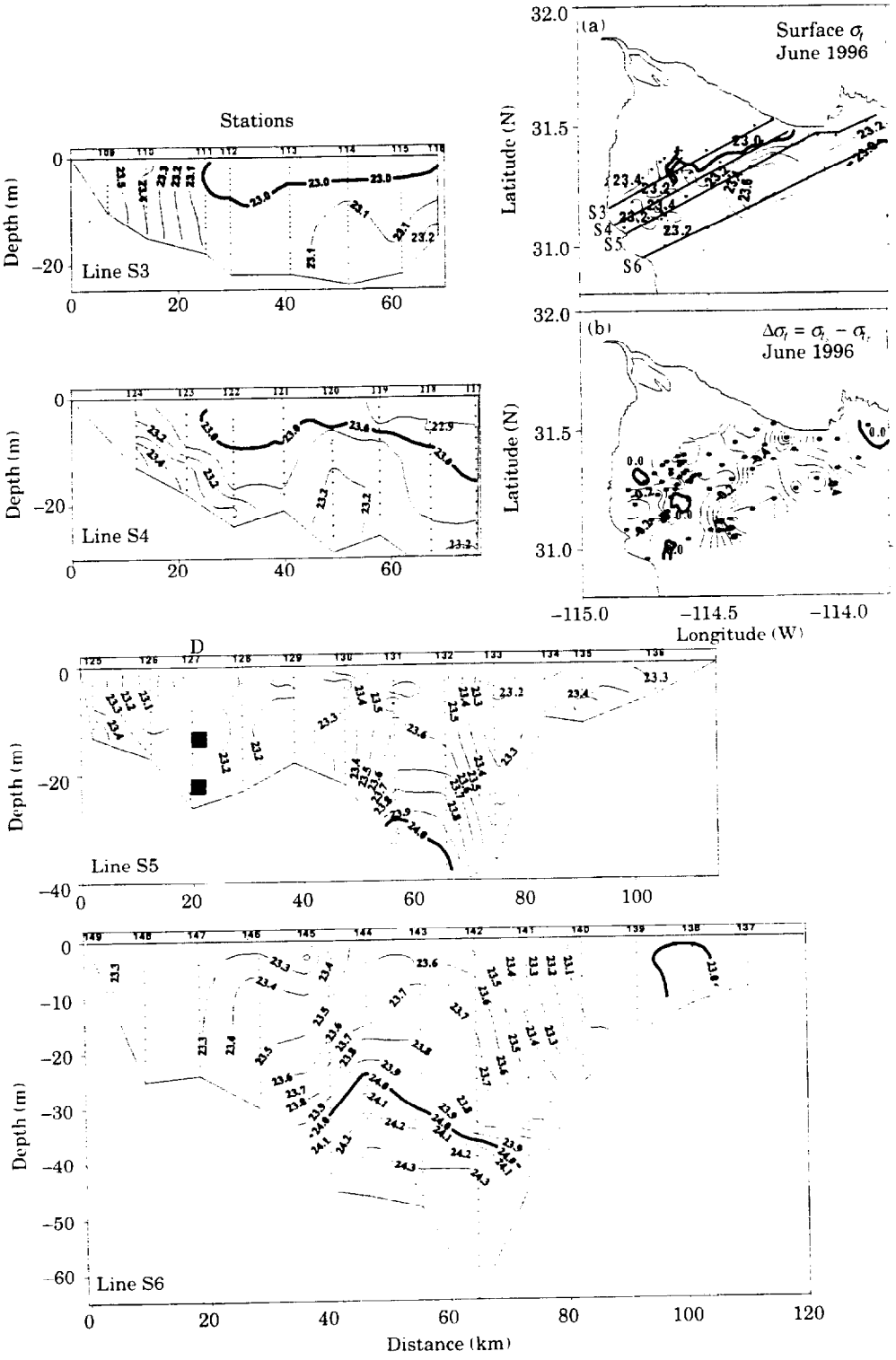

FIGURE 12. Distribution of σ_t in the Upper Gulf of California in June, 1996: (a) surface σ_t; (b) surface to bottom σ_t difference. Line S3 to Line S6: vertical cross-sections of σ_t along the cross-gulf lines marked in (b). The black squares in Line S5 (Site D) show the position of the current meters.

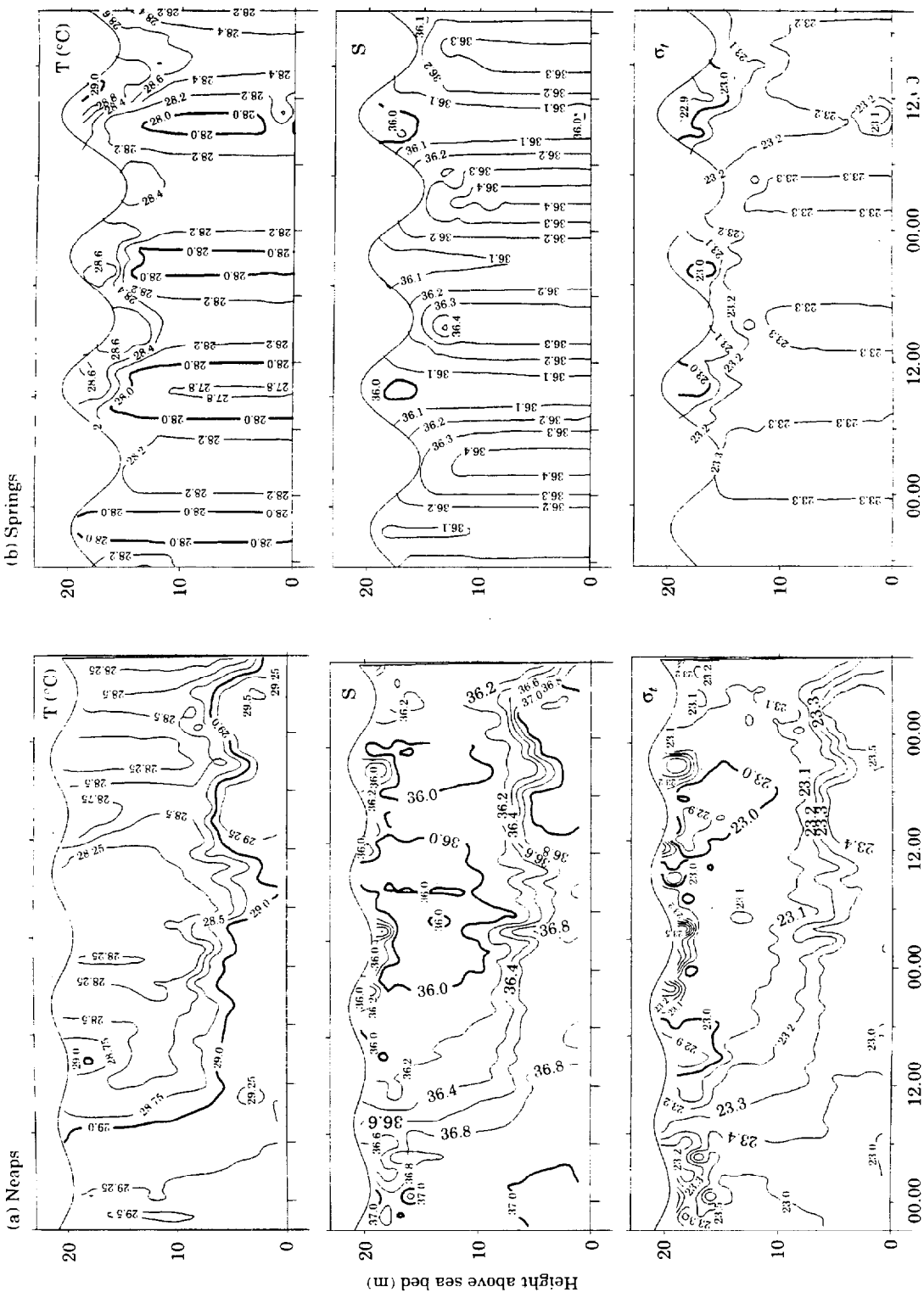

FIGURE 13. Time-series of CTD casts, made at site D, simultaneously with the current meter measurements of the next Figure (24–25 June 1996). On the left (a), the data for neaps tides shows very strong temperature and salinity inversions. On the right (b), the data for spring tides shows vertically mixed conditions.

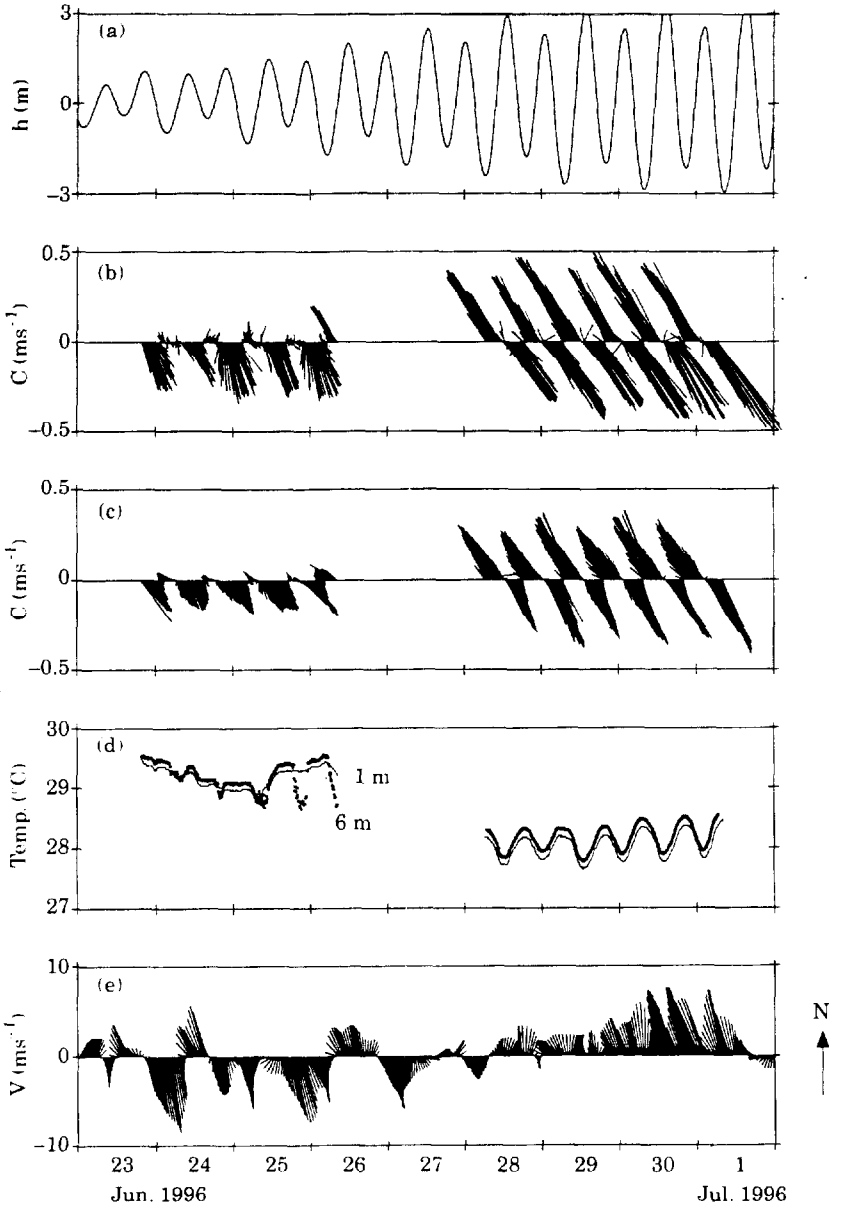

FIGURE 14. Time-series of sea level, currents and wind, made simultaneously with the current meter measurements of Figure 13 (24–25 June 1996): (a) sea level at San Felipe; (b) current vectors 6 m above the bottom at Site D; (c) current vectors 1 m above the bottom at Site D; (d) temperature at 1 and 6 m above the bottom at Site D; (e) wind vectors measured at Punta Estrella, drawn in oceanographic convention.

$S \approx 36{\cdot}0$, $\sigma_t \approx 23{\cdot}0$), while the properties of the initial homogeneous water are now found only in a 7 m-thick bottom layer. During the stratified period, which lasted for at least 40 h, salinity and temperature stratification were 0·4 and 0·6 °C, respectively, with $\Delta\sigma_t$ of about 0·4.

The current meter data collected at the same time as the neaps CTD time-series [Figure 14(a)] show that a residual current to the South completely arrests the flood tidal current [Figure 14(b) and (c)], both at 1 and 6 m above the bottom; the average speed over 2 tidal cycles is $\sim 0{\cdot}1$ ms^{-1}. More accurate estimates of the residual current can be obtained with Progressive Vector Diagrams, or by low-pass filtering the data shown in Figure 14(b) and 14(c), either filling the gaps with zeros or with predicted tidal currents; the results do not differ significantly at the centre of the sampled period. At 1 m above the bottom, the current is toward 141°, at 0·102 ms^{-1}; at 6 m above the bottom, the direction is 154° and the speed is

$0{\cdot}125\ \mathrm{ms}^{-1}$. The 13° difference in direction suggests a bottom Ekman layer. The temperature records from the current meters [Figure 14(d)] show that at times the upper current meter was above the homogeneous bottom layer, as evidenced by the short-time pulses of temperature lower than at 1 m; this is congruent with the presence of internal waves in the pycnocline, which can be seen in the concurrent CTD data [Figure 13(a)].

The springs CTD time-series [Figure 13(b)] show almost well-mixed conditions, with $T \approx 28\ ^\circ\mathrm{C}$, $S \approx 36{\cdot}3$ and $\sigma_t \approx 23{\cdot}3$. There seems to be day-time near surface temperature stratification due to solar radiation. The currents measured during the spring tides [Figure 14(b) and (c)] reach up to $0{\cdot}5\ \mathrm{ms}^{-1}$, and are responsible for the almost well-mixed conditions. The average speed over five tidal cycles is very slow ($\sim 0{\cdot}01\ \mathrm{ms}^{-1}$). The mean shear between 1 and 6 m above the bottom is $\sim 0{\cdot}02\ \mathrm{s}^{-1}$. The current meters show that the temperature structure is now stable [Figure 14(d)], that it has fallen from $\sim 29\ ^\circ\mathrm{C}$ to $\sim 28\ ^\circ\mathrm{C}$ since the neaps observations, and that it has a tidal signal of $0{\cdot}2\ ^\circ\mathrm{C}$ amplitude; all this is in agreement with the concurrent CTD data [Figure 13(b)].

The data suggest that during this summer survey a water-mass formation event was witnessed, and that the dense water formed in the region moved as a 7 m-thick bottom gravity current with speeds of about $0{\cdot}1\ \mathrm{ms}^{-1}$. This occurred during neap tides only, probably because the intense tidal stirring during spring tides inhibits the formation of a two-layer structure, and destroys that formed during neap tides. The neaps CTD time-series [Figure 13(a)] clearly shows the shape of the intruding head of lighter fluid in the upper layers; the bottom head of dense fluid does not show because the CTD data were taken on the warm, salty side of the (originally vertical) density front.

High summer (1–7 August 1995). As the T/S diagram [Figure 4(b)] shows, in this cruise was found the warmest, saltiest and least dense water. The surface salinity [Figure 15(a)] reaches 38·2 in the NW, while in the deeper central part, 35·4 salinity indicates the presence of water typical of Wagner Basin; in Adair Bay salinity rises again (36·4). The shape of the surface isohalines off the BC side suggest a tongue of the high salinity coastal water flowing South along the isobaths; in this area, the bottom salinity is higher than at the surface by about 0·2 [Figure 15(b)]. There is a central area in the UGC where S is vertically homogeneous [Figure 15(b)], but in most of it $\Delta S < 0$, while in Wagner Basin ΔS reaches 0·4. The vertical distribution of salinity (Lines S1 to S6, Figure 15) shows a zone of salinity maximum that starts in the shallowest NW area and extends slightly offshore all the way to section S6, where it is found in Station 5 as a subsurface nucleus of $S \approx 36$ at a depth of 20 m. From S4 to S6, the deeper area is occupied with water from Wagner Basin, with $S \approx 35{\cdot}4$. Salinity is high (>36) in Adair Bay, and again there is the suggestion, by the shape of the isohalines between Stations 25 and 26 (Line S5), that the S maximum at the bottom of Station 42 (Line S4) may have originated in Adair Bay.

The surface isotherms [Figure 16(a)] run across the axis of the UGC, except in the edge of Wagner Basin, where they follow the bathymetry. The warmest water (>32 °C) is in the NW side and in Adair Bay. Colder water lies at the bottom ($\Delta T \approx 0{\cdot}2\ ^\circ\mathrm{C}$), except in Adair Bay. [Figure 16(b)]. The vertical sections of temperature (Lines S1 to S6, Figure 16) clearly show the presence of Wagner Basin stratified water in the deeper part of the southernmost sections. The salinity maximum at the bottom of Station 5 (Line S6, Figure 16) does not have an associated temperature anomaly.

The surface density [Figure 17(a)] was about 22 in most of the UGC and in Adair Bay. The NW area again stands out, with a maximum of 23·2, and a suggestion of a southward-flowing tongue of dense water, clearly reflecting the salinity distribution [Figure 15(a)]. Stable conditions were found throughout the UGC [Figure 17(b)], with $\Delta\sigma_t \approx 0{\cdot}1$. The vertical sections of density (Lines S1 to S6, Figure 17) follow those of salinity on the western side. The shadings in Figure 17 show the distribution of the water with $22{\cdot}3 \leq \sigma_t \leq 22{\cdot}6$ (light shading) and $22{\cdot}6 \leq \sigma_t \leq 23{\cdot}0$ (dark shading), illustrating that the density that corresponds to the salty water in the NW is found outside the UGC at a depth of ~ 20 m. The core of high salinity, isothermal water found in Station 5 (Line S6, Figure 15) seems to have been generated close to the head, since its density (22·7) is present from Line S1 to Line S3 (Figure 17).

Discussion

Water-mass formation and gravity currents

Recent studies on water-mass formation in the Northern Gulf of California (Lavín *et al.*, 1995; López, 1997) suggest that the high-salinity water that is found in winter at the bottom of Wagner Basin comes from shallow areas like the UGC and Adair Bay, and that upon leaving the formation area, the newly formed water moves as a gravity current along

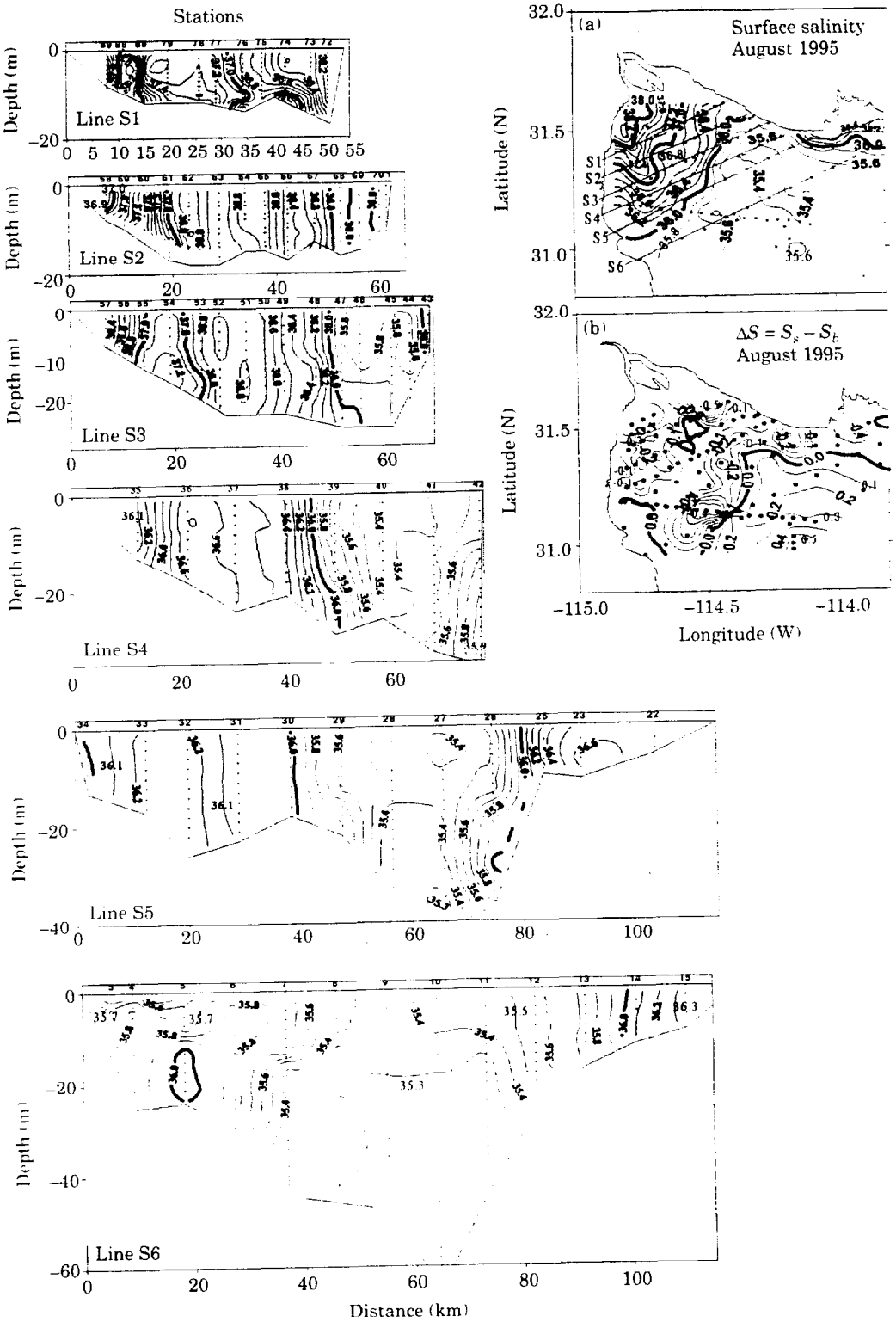

FIGURE 15. Distribution of salinity in the Upper Gulf of California in August 1995: (a) surface salinity; (b) surface to bottom salinity difference. Line S1 to Line S6: vertical cross-sections of salinity along the cross-gulf lines marked in (a).

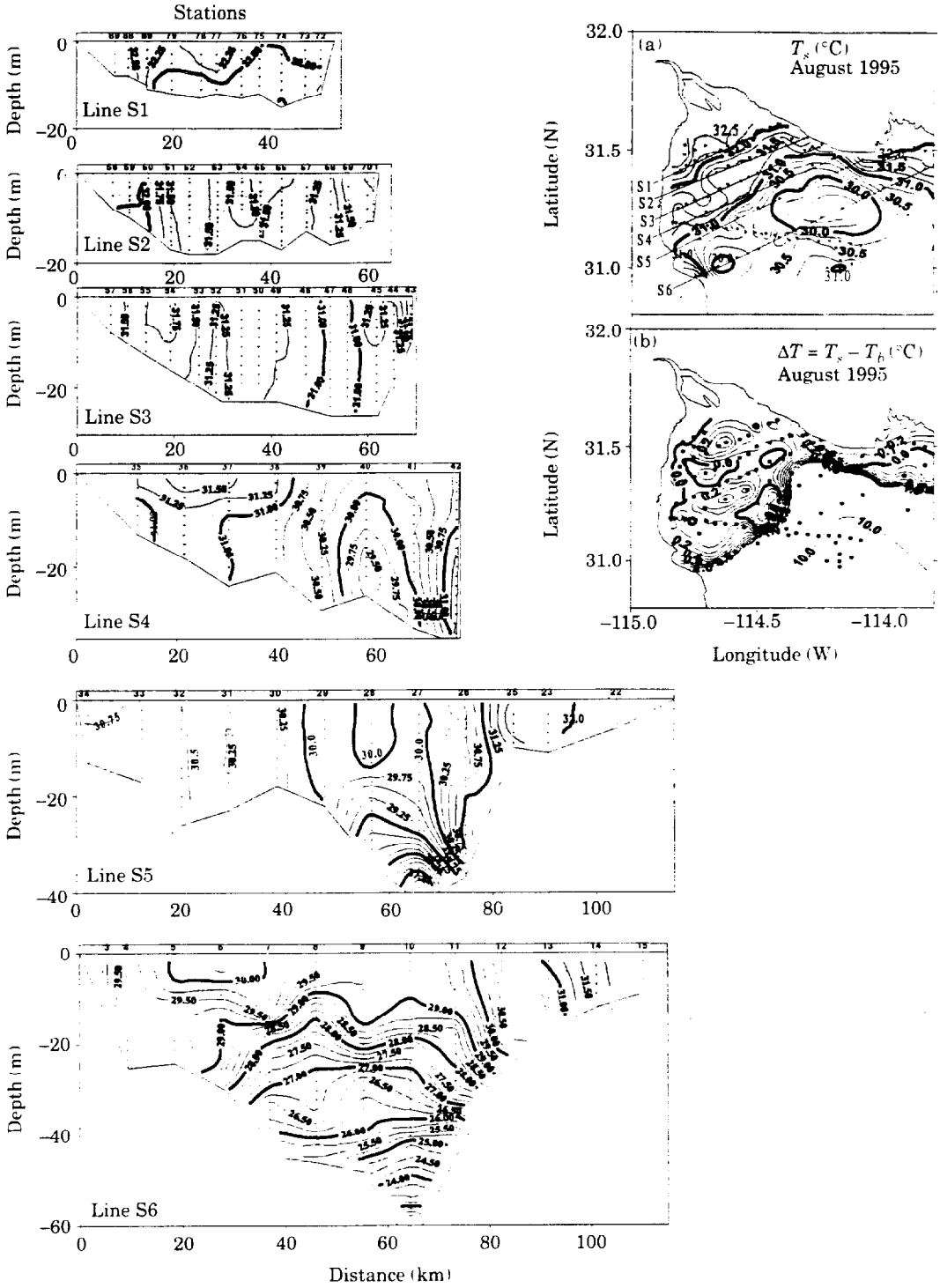

FIGURE 16. Distribution of temperature in the Upper Gulf of California in August 1995: (a) surface temperature; (b) surface to bottom temperature difference. Line S1 to Line S6: vertical cross-sections of temperature along the cross-gulf lines marked in (a).

the isobaths, with the shallow water to the right of the motion. However, no observational or numerical studies of water mass formation have hitherto been performed on the UGC proper.

In the T/S diagrams of the UGC (Figure 4), for all months there are isopycnals that cross the T/S diagrams at two places. The isopycnal that touches the tip of the high-salinity end of the diagram crosses it again

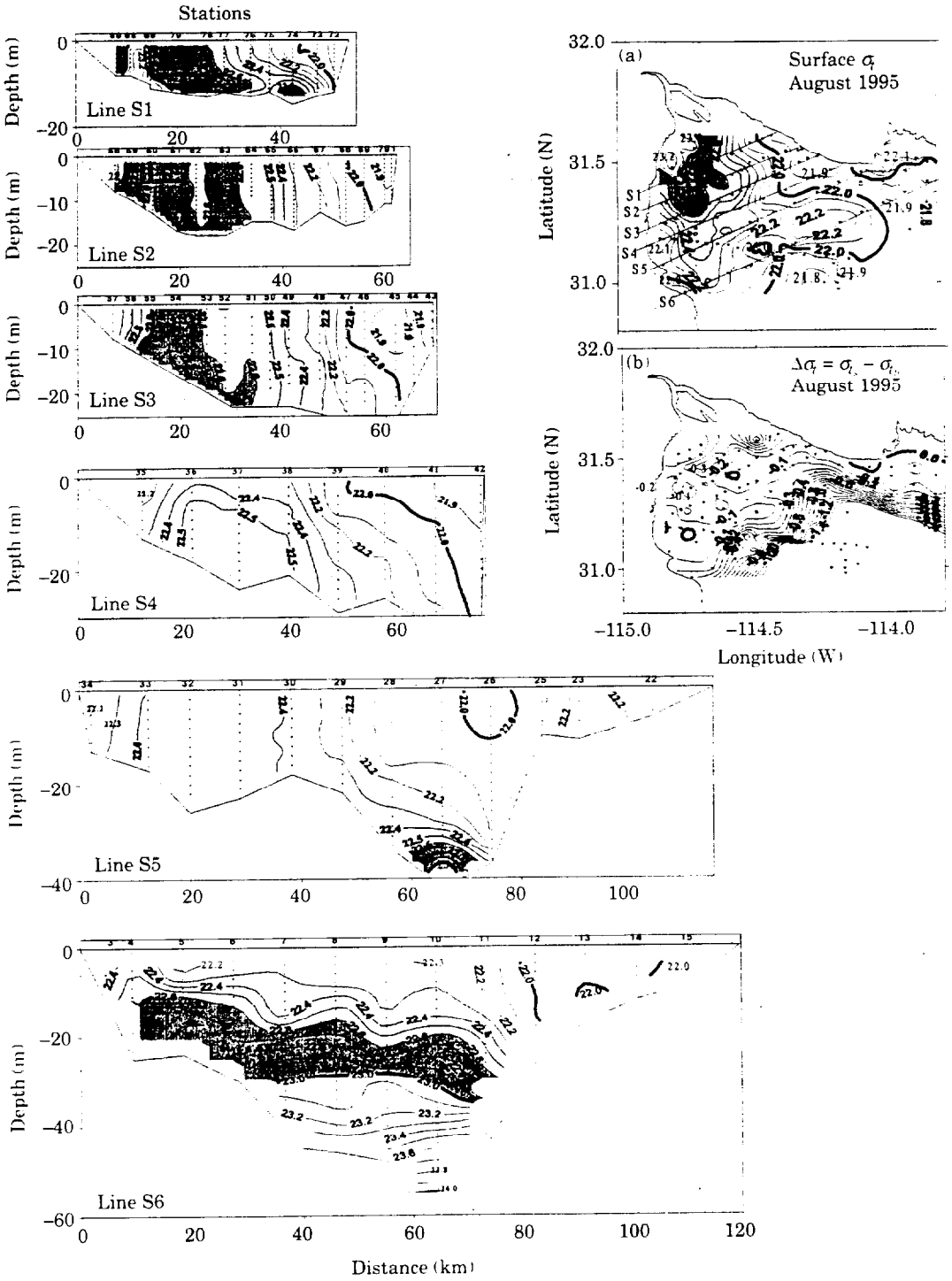

FIGURE 17. Distribution of σ_t in the Upper Gulf of California in August 1995: (a) surface σ_t; (b) surface to bottom σ_t difference. Line S1 to Line S6: vertical cross-sections of σ_t along the cross-gulf lines marked in (b).

at a place, which is below the surface, where the salty water from the UGC would find its equilibrium position (in the absence of entrainment) after going through the process of convection. The phenomenon has been documented in the Northern Gulf for winter (Alvarez-Borrego & Schwartzlose, 1979; Lavin *et al.*, 1995), but the possibility of its occurrence in summer, suggested by Figure 4, had not been considered before.

Water-mass formation is a widespread phenomenon in high latitudes, and it also occurs in a few

TABLE 2. Characteristics of the Upper Gulf of California and the South Australian Gulfs

	Upper Gulf of California[a]	Spencer Gulf[b]	Gulf St Vincent[c]
Area (km^2)	4500	19 500	7000
Mean depth (m)	20	22	25
Latitude	31°N	32°S	33°S
E ($m\ year^{-1}$)	1·1	1·0	1·7
Tidal currents	M_2=0·28	M_2=0·09	M_2=0·25
major semiaxis	S_2=0·21	S_2=0·10	S_2=0·27
(ms^{-1})	K_1=0·03	K_1=0·22	K_1=0·05
	O_1=0·02	O_1=0·11	O_1=0·04
Wind (ms^{-1})	Winter 8–12	Winter 3–10	Winter 3–10
	Summer 2–6	Summer 3–10	Summer 3–9
Head	Summer 33	Summer 24	Summer 24
T (°C)	Winter 8	Winter 12	Winter 13
Head	Summer 40	Summer 48	Summer 42
S	Winter 36	Winter 43	Winter 39
Head	Summer 29·2	Summer 33·0	Summer 28·8
σ_t	Winter 23·5	Winter 33·5	Winter 29·7
Mouth S	35·4	35·9	36·5
$\partial\rho/\partial y$ (kgm^{-4})	$2–6 \times 10^{-5}$	5×10^{-5}	$4\ 10^{-5}$

[a]Data from: Alvarez Borrego *et al.* (1973), and this publication.
[b]Data from: Nunes-Vaz *et al.* (1990) and references therein. Also pers. comm. R. Nunes-Vaz (1998).
[c]Data from: Provis and Lennon (1983), de Silva Samarasinghe and Lennon (1987), de Silva Samarasinghe (1989).

semi-enclosed seas, like the Mediterranean, the Red Sea and the Adriatic, where evaporation produces very high salinities. However, the conditions of the UGC are most similar to those of the South Australian gulfs (see Table 2), where the physics of warm-water inverse estuaries has been extensively investigated (see: Nunes Vaz *et al.*, 1990, and references therein). In these inverse estuaries, gravity currents generated by the water-mass formation process are a very important component of the regional oceanography.

Gravity currents in inverse estuaries are due to the pressure gradient induced by the increase of density toward the head: the dense, salty water slips under (and is replaced at the surface by) the lighter offshore water. Initially, the gravity current is in the direction of the pressure gradient, being affected only by friction with the bottom and the surrounding water: the water flows downslope across the isobaths, seeking the depth where the surrounding water has the same density. Within a time scale of $2\pi/f$ (~ 1 day in the UGC, equivalent to a length scale of ~ 10 km), the gravity current should be deviated to the right (in the Northern Hemisphere) by Coriolis force. When geostrophic balance is achieved, the flow is along the isobaths with the shallow water to the right of the motion. Friction induces cross-isobath motion, and the water keeps sinking until its density matches that of the surroundings (see Griffiths, 1986; or Bowers, 1989, and references therein).

Summer The current meter and CTD time-series collected during neap tides in June 1996 (Figures 14 and 13) show the evolution of a density current, with an estimated speed of $\sim 0{\cdot}1\ ms^{-1}$. This speed is much stronger than those estimated with numerical models for wind forcing ($0{\cdot}01–0{\cdot}03\ ms^{-1}$; Argote *et al.*, 1998), and for tidal rectification ($\sim 0{\cdot}01\ ms^{-1}$, Marinone, 1997; Argote *et al.*, 1998).

The relationship between the bottom density distribution, the gravity current and the bathymetry is shown in Figure 18. The residual flow is approximately normal to the bottom isopycnals, and its angle with the local bathymetry is about 7° at 6 m and 21° at 1 m above the bottom.

The steady-state equations for a gravity current in a *uniformly sloping bottom* are (Bowers & Lennon, 1987):

$$\text{Along-flow balance:} \quad g'\alpha \sin() = ku^2/h \qquad (1)$$

$$\text{Across-flow balance:} \quad g'\alpha \cos() = fu, \qquad (2)$$

where u is the speed of the gravity current, f is the Coriolis parameter ($7{\cdot}29 \times 10^{-5}\ s^{-1}$ at 31 °N), g' is the reduced gravity, h is the thickness of the layer, α is the slope of the interface (which is also the bottom

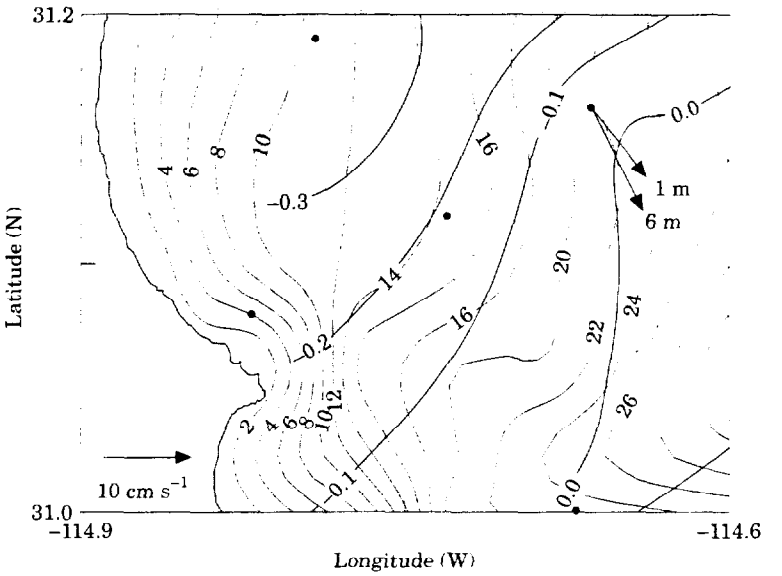

FIGURE 18. Relationship between gravity current, density structure and bathymetry in June 1996. Arrows are the residual currents at Site D during neap tides. The thin contours are the bathymetry in metres, and the thick contours are bottom σ_t. The small dots are the CTD stations.

slope), Θ is the angle between the current and the isobaths and k is a friction coefficient ($\sim 0{\cdot}006$; according to Bowers & Lennon, 1987). The two equations allow the calculation of two of the three parameters u, k or Θ, given the other one.

Although the CTD survey was made (immediately) after the neaps RCM measurements, let's assume that the gravity current was generated by a density distribution not very different to that shown in Figure 12. From the density cross-section at Line S4, Figure 12: $g' = 4 \times 10^{-3} \mathrm{ms}^{-2}$, $h = 7$ m [see also Figure 13(a)], $\alpha = 20$ m/20 km $= 10^{-3}$. Taking $\Theta \approx 15°$ (the calculation is not very sensitive to Θ), the geostrophic balance (2) gives $u = 0{\cdot}053$ m s^{-1}, which is in reasonable agreement with the observations. Since k is the most poorly known parameter, Equation 1 and the measured values of u and Θ can be used to calculate that $k = 0{\cdot}0026$.

These orders of magnitude are encouraging, but we don't have enough information to establish how close to geostrophic balance the situation was during sampling. This is determined from Θ; for instance, before geostrophic balance is reached, the flow is across the isobaths ($\Theta = \pi/2$), and the along-current equation becomes $u = (g' h\alpha/k)^{1/2}$. With $k \approx 0{\cdot}003$, $u \approx 0{\cdot}10$ ms^{-1}, which is very close to the observed residual currents. Unfortunately, as Line S5 Figure 12 shows, the current meters were in a bathymetric depression, which may have affected the observed direction of the gravity current. This doesn't allow a good comparison with the simple theory presented above. It is clear that a better data set is needed.

By the time CTD and current meter time-series were resumed during spring tides (Figures 13 and 14), the T and S inverted conditions had disappeared and there was no strong residual flow (the average over 5 tidal cycles is only $0{\cdot}01$ ms^{-1}). It is proposed that the hydrographic conditions and the gravity current observed during neap tides disappear during spring tides due to the increased vertical mixing. The formation of gravity currents in inverse estuaries and their inhibition by vertical mixing have been studied in the laboratory (Linden & Simpson, 1986, 1988; Simpson & Linden, 1989) and their presence in nature has been documented in the South Australian Gulfs (de Silva Samarasinghe & Lennon, 1987; Nunes & Lennon, 1987; de Silva Samarasinghe, 1989; Nunes Vaz *et al.*, 1989, 1990). In these gulfs, neap tidal currents are very small and $\Delta\sigma_t$ reaches $-1{\cdot}0$; if the neap tides and calm coincide, the dense water in the interior of the gulf flows out, reaching a geostrophic balance with current speed of $\sim 0{\cdot}1$ ms^{-1}. In the Australian gulfs this occurs in both winter and summer (Nunes & Lennon, 1987), but the effects are more clearly seen and the gravity current reaches much farther and deeper during autumn and winter (Lennon *et al.*, 1987; Nunes Vaz *et al.*, 1990).

In summary, the summer observations show that vertical convection occurs during summer in the shallowest part of the UGC, that gravity currents are generated, and that they may be fortnightly modulated. None of these phenomena had been reported before for summer–autumn in the UGC.

TABLE 3. Properties of the surface and bottom water in Wagner Basin, for selected winter–spring cruises

Cruise→	Dec. 1993	Dec. 1994	Jan. 1990	Jan. 1995	Mar. 1973	Mar. 1988	Mar. 1996
S_s	35·60	35·47	35·45	35·41	35·35	35·31	35·50
S_b	34·97	**36·14**	35·15	**35·61**	**35·50**	**35·50**	35·00
T_s (°C)	19·30	18·18	16·50	16·74	16·50	15·00	19·50
T_b (°C)	13·47	17·20	14·00	16·16	15·00	14·67	13·50
σ_{ts}	25·41	25·59	25·97	25·89	25·90	25·90	25·20
σ_{tb}	26·28	26·34	26·30	26·18	26·45	26·41	26·30
$\sigma_{ts}-\sigma_{tb}$	− 0·87	− 0·78	− 0·33	− 0·29	− 0·45	− 0·51	1·10

Surface values with s subindex; Bottom (200 m) values with b subindex. Bottom salinities in **bold** type indicate the cases when the salinity at the bottom of Wagner Basin was higher than at the surface.

Winter-Spring The two previously reported observations of winter high-salinity water in the bottom of Wagner Basin (Alvarez-Borrego & Schwartzlose, 1979; Lavín *et al.*, 1995), presumably originating in the UGC, both occurred during the month of March, which may suggest that March is the month in which the most extensive convection occurs in the UGC. But there have been March data showing no extensive water mass formation; e.g. 1939 and 1985 (Sverdrug, 1941; Bray, 1988). In addition, the T/S diagrams of the UGC show (Figure 4) that by March the temperature of the UGC is several degrees above the winter minimum, and its density has decreased correspondingly. Also, by March the surface heat flux in the UGC has become positive (Reyes & Lavín, 1997). The apparent rapid thermal response of the UGC may be due to the shallowness of the area, and also to the flushing generated by the gravity currents.

The surface and bottom values of salinity, temperature and σ_t in Wagner Basin as measured in cruises between December and March are shown in Table 3. The Wagner Basin bottom water of coastal origin had temperature just under 15 °C in March 1988, and about 16·5 °C in March 1973; in both occasions salinity was about 35·5, and σ_t exceeded 26·3. In March 1996, no high-salinity bottom water was found in Wagner Basin: although high salinity was present in the UGC (>36, Figure 6), the water was not dense enough to sink to the bottom of Wagner Basin because its temperature was high (T ~ 19·5 °C, Figure 7). However, high salinity bottom water was found in Wagner Basin in December 1994 and January 1995 (Table 3): this is the first reported occurrence of the phenomenon in months different from March.

As Table 3 shows, there is much variability in the properties (T, S, σ_t) of the high-salinity water that reaches the bottom of Wagner Basin. A possible explanation for this variability is as follows: water-mass formation takes place throughout the year, with (sporadic) gravity currents taking the high-salinity water out of the UGC at a greater and greater depth as the seasons progress from summer to winter and the density of the formed water increases as shown, e.g. in the T/S diagrams (Figure 4). Evidence for this is the frequent presence (in CTD casts taken in Wagner and Delfin Basins) of mid-depth layers of high salinity, as reported by Bray (1988), by Lavín *et al.* (1995) and by López (1997)).

However, because of the shallowness of the UGC, the density of the water responds strongly to variability in the surface heat losses; this variability is controlled by the meteorology, which in turn has wide interannual variations (Reyes & Lavín, 1997). Therefore the month in which water is formed (and its T, S and σ_t) with high enough density to reach the bottom of Wagner Basin probably depends on the meteorology. The evidence presented here suggests that March may not be the month in which the phenomenon occurs most years. The surface fluxes of heat and moisture and the seasonal cycles of temperature and salinity (Figure 4) favour the months of December to February, which are the months in which density is maximum, but the year to year variations can be very wide.

Although no data are available from October and November, the T/S diagrams (Figure 4) indicate that these are the months when the annual salinity maximum (reached in August) is flushed from the top of the UGC. It is possible that the most extensive gravity current flushing takes place at this time, when the extremely salty water is cooled. But since it is still warm, its density is not high enough to reach the bottom of Wagner Basin, and remains in mid-depth layers.

Stratification

In the hydrographic observations in grids of stations and in the CTD time-series, slight stratification was present, with $\Delta\sigma_t \approx -0{\cdot}2$, except in winter [Figure 5(f)]. The presence of this slight, probably sporadic, stratification seems to be in disagreement with the prediction by Argote *et al.* (1995) that the UGC should be well-mixed throughout the year; it is a question of time-scales and non-parameterized phenomena. For instance, the largest observed stratification $\Delta\sigma_t \approx -0{\cdot}4$, occurred during the neaps CTD time-series of June 1996 [Figure 12(a)], but as explained before, it was due to the subsurface gravity current of high salinity.

The analysis of Argote *et al.* (1995) is an energy balance in a time-scale of months, of the mixing tendency due to the M_2 tidal currents and the stratifying tendency due to surface heating. The apparent widespread presence of slight stratification [Figures 8(b), 12(b) and 17(b)] in the UGC may be due to the fact that most of the CTD stations were made during neap tides. Apart from the neap-tides stratification associated with the gravity currents, diurnal thermoclines can be formed close to the surface at the times of maximum insolation (Figure 13).

Through direct straining of the horizontal density field, vertical shear in the tidal currents can introduce periodic stratification, depending on the horizontal density gradient and the vertical gradient and intensity of the tidal currents (Simpson *et al.*, 1990; Nunes Vaz & Simpson, 1994). From the current meter observations made at 1 and 6 m above the bottom in the spring tides between June 28 and July 1, 1996 (Figure 14), the mean vertical shear is calculated at $0{\cdot}02\ s^{-1}$. If it is assumed that the vertical profile is given by (Bowden & Fairbairn, 1952) $u(z) = 1{\cdot}15-0{\cdot}425(zh^{-1})^2$, the amplitude of the difference between 1 m above the bottom and the surface is $0{\cdot}2\ ms^{-1}$. This is equivalent to a surface tidal excursion of 1·5 km, relative to 1 m above the bottom. The horizontal gradients of σ_t in the zone [Figure 12(a)] are of order 0·2/10 km; therefore, no significant stratification can be introduced by this mechanism.

Geographic distribution and circulation

The most obvious feature of the horizontal distribution of the hydrographic variables T, S and σ_t is the tendency for the extreme values to occur in the NW of the UGC: all the surface distributions show isolines with a N or NNE orientation, in both data sets. This was noted by Alvarez-Borrego and Galindo-Bect (1974), who proposed that it was an indirect evidence of a cyclonic residual circulation in the UGC. Although this is a reasonable proposition, inferring residual circulation from horizontal distributions of properties can lead to erroneous conclusions under certain circumstances (Hunter, 1975). In the case of the UGC, the inference certainly deserves close scrutiny, since the isolines also seem to reflect the bathymetry. In the similar case of the South Australian Gulfs, the distribution of salinity departs markedly from the bathymetry pattern (Nunes & Lennon, 1986); in this case the geographic distribution of variables has been proved by direct current measurements to be caused by the residual circulation (Nunes Vaz *et al.*, 1990).

The western, peninsular side of the UGC is much shallower, the bottom slope is much gentler, and it is farther from Wagner Basin than the SE part. This alone can explain the distributions, without recourse to a residual circulation; given a rate of evaporation E and a surface heat flux Q, the change of salinity (δS) and temperature (δT) in a time interval δt is larger the shallower the depth of the water column (h), since $\delta T = Q\delta t/(\rho C_p h)$, and $\delta S = SE\delta t h^{-1}$ (where ρ is the density and C_p is the specific heat of water). Therefore the isotherms and isohalines will follow the isobaths, with extreme values in the shallowest water. The eastern side of the entrance not only is deeper and the bottom slope very pronounced off the mainland coast, but Wagner Basin is a large reservoir of relatively low salinity (<35·4), which can be diffused laterally and vertically. The distribution of the low salinity water follows the depth contours in this area, and the distributions of salinity across the entrance to the UGC clearly show the presence of water from Wagner Basin [Figures 5(b), 6, 10 and 15]. However, the isolines are not exactly parallel to the isobaths, and the small difference could be due to residual circulation. In Figures 10 and 15 the trend of the isohalines seem to reflect the gravity currents.

Conclusions

Like other negative estuaries, in the UGC the salinity increase toward the head causes the density to do likewise; this occurs throughout the year, despite the seasonally reversing temperature gradient. The pressure gradient thus formed leads to gravity currents: in the case observed, the dense, salty water slipped under the lighter offshore water as a 7 m thick bottom layer at a speed of $\sim 0{\cdot}1\ ms^{-1}$. The gravity currents appear to be modulated by the available TKE, mainly form the tidal currents, but wind stirring is likely to be of importance. These currents, although

sporadic, are significantly faster than the wind-induced and tide-induced residuals, and they occur precisely when the tides and the winds are at their weakest.

Evidence of summer water mass formation in the UGC is presented here for the first time. While in winter water with the same density (σ_t>26) as that formed in the UGC is found south of Wagner Basin at depths exceeding 200 m (Lavín *et al.*, 1995), in summer water with $\sigma_t \sim 23{\cdot}4$ is found near the entrance to the UGC at a depth of only 20–30 m (Figures 15 and 17).

The results presented here confirm that the UGC is the source of the high-salinity water that is frequently found during winter at the bottom of Wagner Basin and further south. Adair Bay was also seen to produce high-salinity bottom water, and some salty bottom water may also be formed in the shallow shelf (<30 m deep) off mainland México.

In the vertical dimension, slight stratification $\Delta\sigma_t \approx O(-0{\cdot}2)$ was encountered in most of the surveys, which were made in neap tides. It is proposed that this stratification is sporadic, due to vertical convection of coastal dense water, and to solar radiation. Shearing stress of the tidal currents seems to be unimportant in generating periodic stratification.

Although limited, the data provide tantalising evidence of mixing-modulated gravity currents, but longer time-series and more detailed studies of the structure and properties of these currents are needed.

Acknowledgements

This work was funded by CICESE, and by CONACYT through Contracts No. 25555-T9712 and 3007P-T9606, and a postgraduate scholarship for Victor M. Godínez. This paper was finished during a sabbatical stay at School of Geography and Oceanography, ADFA, University of New South Wales, Canberra, Australia, with support from ADFA, CONACYT and CICESE. The authors want to thank the enthusiastic support of the crew of the RV *Francisco de Ulloa*, and the field and cabinet efforts of Carlos Cabrera, Emilo Palacios and Salvador Sánchez.

References

Alvarez-Borrego, S., Galindo-Bect, L. A. & Flores-Báez, B. P. 1973 Hidrologia. En *Estudio Quimico Sobre la Contaminación por Insecticidas en la Desembocadura del Rio Colorado*. Tomo II. Reporte Final a la Dirección de Acuacultura de la Secretaria de Recursos Hidraulicos. Universidad Autónoma de Baja California. 248 pp.

Alvarez-Borrego, S. & Galindo-Bect, L. A. 1974 Hidrologia del Alto Golfo de California-I. Condiciones durante otoño. *Ciencias Marinas* **1**, 46–64.

Alvarez-Borrego, S., Flores-Báez, B. P. & Galindo-Bect, L. A. 1975 Hidrologia del Alto Golfo de California II. Condiciones durante invierno, primavera y verano. *Ciencias Marinas* **2**, 21–36.

Alvarez-Borrego, S. & Schwartzlose, R. 1979 Water masses of the Gulf of California. *Ciencias Marinas* **6**, 43–63.

Alvarez Sánchez, L. G., Godinez, Victor. M., Lavín, M. F. & Sánchez, S. 1993 Patrones de turbidez y corrientes en la Bahia de San Felipe, al NW del Golfo de California. *Communicaciones Académicas CICESE*, CTOFT-9304, 48 pp.

Argote, M. L., Amador, A., Lavín, M. F. & Hunter, J. R. 1995 Tidal dissipation and stratification in the Gulf of California. *Journal of Geophysical Research* **100**, 16103–16118.

Argote, M. L., Lavín, M. F. & Amador, A. 1998 Barotropic residual circulation in the Gulf of California due to the M_2 tide and wind stress. *Atmósfera* **11**, 173–197.

Beier, E. 1997 A numerical investigation of the annual variability in the Gulf of California. *Journal of Physical Oceanography* **27**, 615–632.

Bowden, K. F. & Fairbairn, L. A. 1952 A determination of the frictional forces in a tidal current. *Proceedings of the Royal Society of London, Series A* **214**, 371–392.

Bowers, D. G. & Lennon, G. W. 1987 Observations of stratified flow over a bottom gradient in a coastal sea. *Continental Shelf Research* **9**, 1105–1121.

Bowers, D. G. 1989 Models of density current outflows from inverse estuaries: with application to Spencer Gulf, South Australia. In *Focus on Modelling Marine Systems Vol. 2* (Davies, A. M., ed.). CRC State-of-the-art series on numerical Modelling of Marine Systems, pp. 1–23.

Bray, N. 1988 Water mass formation in the Gulf of California. *Journal of Geophysical Research* **93**, 9223–9240.

Carbajal, N. 1993 *Modelling of the Circulation in the Gulf of California*. PhD. thesis, Institute of Oceanography, University of Hamburg, 186 pp.

Carbajal, N., Souza, A. & Durazo, R. 1997 A numerical study of the ex-ROFI of the Colorado River. *Journal of Marine Systems* **12**, 17–33.

Castro, R., Lavín, M. F. & Ripa P. 1994 Seasonal heat balance in the Gulf of California. *Journal of Geophysical Research* **99**, 3249–3261.

de Silva Samarasinghe, J. R. & Lennon, G. W. 1987 Hypersalinity, flushing and transient salt-wedges in a tidal gulf-an inverse estuary. *Estuarine, Coastal and Shelf Science* **24**, 483–498.

de Silva Samarasinghe, J. R. 1989 Transient salt-wedges in a tidal gulf: a criterion for their formation. *Estuarine, Coastal and Shelf Science* **28**, 129–148.

Garcia Córdoba, J., Robles, J. M. & Flores Cabrera, C. F. 1995 Datos de CTD obtenidos en la Bahia de Todos Santos, B. C. Campaña BATOS 4. B/O Francisco de Ulloa. Marzo 22–24 de 1994. *Comunicaciones Académicas, Serie Oceanografia Fisica No. CTOFT9506*. CICESE, Ensenada, México. 75 pp.

Godinez, Victor. M., Lavín, M. F. & Sánchez Mancilla, S. 1995 Calibración del CTD Smart en laboratorio y campo. *Communicaciones Académicas, Serie Oceanografia Fisica No. CTOFT9511*. CICESE, Ensenada, México. 14 pp.

Griffiths, R. W. 1986 Gravity currents in rotating systems. *Annual Review of Fluid Mechanics* **18**, 59–89.

Hunter, J. R. 1975 The determination of current velocities from diffusion/advection processes in the Irish Sea. *Estuarine and Coastal Marine Science* **3**, 34–55.

Lavín, M. F., Gaxiola Castro, G., Robles, J. M. & Richter, K. 1995 Winter water masses and nutrients in the northern Gulf of California. *Journal of Geophysical Research* **100**, 8587–8605.

Lavín, M. F., Durazo, R., Palacios, E., Argote, M. L. & Carrillo, L. 1997 Lagrangian observations of the circulation in the Northern Gulf of California. *Journal of Physical Oceanography* **27**, 2298–2305.

Lennon, G. W., Bowers, D., Nunes, R. A., Scott, B. D., Ali, M., Boyle, J., Wenju, C., Hertzfeld, M., Johansson, G., Nield, S., Petrusevics, P., Stephenson, P., Suskin, A. A. & Wijffels, S. E. A. 1987 Gravity currents and the release of salt from an inverse estuary. *Nature* **327**, 695–697.

Linden, P. F. & Simpson, J. E. 1986 Gravity-driven flows in a turbulent fluid. *Journal of Fluid Mechanics* **172**, 481–497.

Linden, P. F. & Simpson, J. E. 1988 Modulated mixing and frontogenesis in shallow seas and estuaries. *Continental Shelf Research* **8**, 1107–1127.

López, M. 1997 A numerical simulation of water mass formation in the northern Gulf of California during winter. *Continental Shelf Research* **17**, 1581–1607.

Marinone, S. G. 1997 Tidal residual currents in the Gulf of California: is the M_2 tidal constituent sufficient to induce them? *Journal of Geophysical Research* **102**, 8611–8623.

Martinez Sepúlveda, M. 1994 *Descripción de la Capa Mezclada Superficial del Golfo de California*. BSc thesis, Facultad de Ciencias Marinas, UABC, Ensenada, México. 48 pp.

Nunes, R. A. & Lennon, G. W. 1986 Physical property distributions and seasonal trends in Spencer Gulf, South Australia: an inverse estuary. *Australian Journal of Marine and Freshwater Research* **37**, 39–59.

Nunes Vaz, R. A., Lennon, G. W. & de Silva Samarasinghe, J. R. 1989 The negative role of turbulence in estuarine mass transport. *Estuarine, Coastal and Shelf Science* **28**, 361–377.

Nunes, R. A. & Lennon, G. W. 1987 Episodic stratification and gravity currents in a marine environment of modulated turbulence. *Journal of Geophysical Research* **92**, 5465–5480.

Nunes Vaz, R. A., Lennon, G. W. & Bowers, D. G. 1990 Physical behaviour of a large, negative or inverse estuary. *Continental Shelf Research* **10**, 277–304.

Nunes Vaz, R. A. & Simpson, J. H. 1994 Turbulence closure modeling of estuarine stratification. *Journal of Geophysical Research* **99**, 16143–16160.

Organista Sandoval, S. 1987 *Flujos de Calor en el Alto Golfo de California*. MSc thesis, CICESE, Ensenada, Mexico. 142 pp.

Provis, D. G. & Lennon, G. W. 1983 Eddy viscosity and tidal cycles in a shallow sea. *Estuarine, Coastal and Shelf Science* **16**, 351–361.

Reyes, A. C. & Lavin, M. F. 1997 Effects of the autumn-winter meteorology upon the surface heat loss in the Northern Gulf of California. *Atmósfera* **10**, 101–123.

Simpson, J. E. & Linden, P. F. 1989 Frontogenesis in a fluid with horizontal density gradients. *Journal of Fluid Mechanics* **202**, 1–16.

Simpson, J. H., Brown, J., Matthews, J. P. & Allen, G. 1990 Tidal straining, density currents and stirring in the control of estuarine stratification. *Estuaries* **12**, 125–132.

Sverdrup, H. U. 1941 The Gulf of California: preliminary discussion of the cruise of the *E. W. Scripps* in February and March 1939. *Proceedings of the 6th Pacific Science Conference*, pp. 161–166.